

**CORRELATIONS BETWEEN MECHANICAL AND
TIME-DEPENDENT PROPERTIES AND
ULTRASONIC PULSE VELOCITY
OF ROCK SALT**



Nisachon Phongklahan

**A Thesis Submitted in Partial Fulfillment of the Requirements for the
Degree of Master of Engineering in Civil, Transportation and
Geo-Resources Engineering
Suranaree University of Technology
Academic Year 2020**

ความสัมพันธ์ระหว่างสมบัติเชิงกลและเชิงเวลาด้วยความเร็วคลื่นดล
อัลตราโซนิกของเกลือหิน



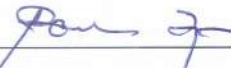
นางสาวนิสาชล พงษ์กล้าหาญ

วิทยานิพนธ์นี้เป็นส่วนหนึ่งของการศึกษาตามหลักสูตรปริญญาวิศวกรรมศาสตรมหาบัณฑิต
สาขาวิชาวิศวกรรมโยธา ขนส่ง และทรัพยากรธรณี
มหาวิทยาลัยเทคโนโลยีสุรนารี
ปีการศึกษา 2563

**CORRELATIONS BETWEEN MECHANICAL AND
TIME-DEPENDENT PROPERTIES AND ULTRASONIC
PULSE VELOCITY OF ROCK SALT**

Suranaree University of Technology has approved this thesis submitted in partial fulfillment of the requirements for a Master's Degree.

Thesis Examining Committee



(Assoc. Prof. Dr. Pornkasem Jongpradist)

Chairperson



(Prof. Dr. Kittitep Fuenkajorn)

Member (Thesis Advisor)



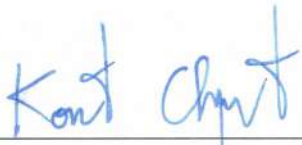
(Asst. Prof. Dr. Akkhapun Wannakomol)

Member



(Dr. Thanittha Thongprapha)

Member



(Assoc. Prof. Ft. Lt. Dr. Kontom Chamniprasart)

Vice Rector for Academic Affairs
and Internationalization



(Assoc. Prof. Dr. Pornsiri Jongkol)

Dean of Institute of Engineering

นิสาชล พงษ์กล้าหาญ : ความสัมพันธ์ระหว่างสมบัติเชิงกลและเชิงเวลาด้วยความเร็วคลื่นอัลตราโซนิกของเกลือหิน (CORRELATIONS BETWEEN MECHANICAL AND TIME-DEPENDENT PROPERTIES AND ULTRASONIC PULSE VELOCITIES OF ROCK SALT) อาจารย์ที่ปรึกษา : ศาสตราจารย์ ดร.กิตติเทพ เฟื่องขจร, 78 หน้า.

การศึกษานี้มีวัตถุประสงค์เพื่อหาความสัมพันธ์ระหว่างความเร็วคลื่นอัลตราโซนิกกับสมบัติเชิงกายภาพและเชิงกล และแรงค์ประกอบของตัวอย่างเกลือหินมหาสารคามภายใต้ปริมาณแร่คาร์บอเนตไลต์และแร่แอนไฮไดรต์ที่แตกต่างกัน การวัดความเร็วคลื่นอัลตราโซนิกดำเนินการโดยใช้ OYO Sonic Viewer 170 (รุ่น 5338) การทดสอบประกอบด้วย 1) การวัดความเร็วคลื่นอัลตราโซนิกเพื่อหาสมบัติแบบไดนามิก 2) การทดสอบการกดในแกนเดียวเพื่อหาสมบัติเชิงกลแบบสถิต 3) การทดสอบการคืบในแกนเดียวเพื่อหาสมบัติการไหลของเกลือ และ 4) การวิเคราะห์การเลี้ยวเบนของรังสีเอกซ์เพื่อระบุแรงค์ประกอบของเกลือหิน ผลการศึกษาพบว่าความหนาแน่นมีผลต่อความเร็วของคลื่น ความแตกต่างของความเร็วคลื่นที่วัดได้อาจเนื่องมาจากการแปรผันของความหนาแน่นของตัวอย่างเกลือหิน ผลการศึกษาแสดงให้เห็นว่าความเร็วของคลื่นปฐมภูมิและคลื่นทุติยภูมิเพิ่มขึ้นตามความหนาแน่น สมบัติเชิงกลและเชิงเวลาและปริมาณแร่แอนไฮไดรต์ที่เพิ่มขึ้น แต่มีค่าลดลงเมื่ออัตราส่วนของปิวของและปริมาณแร่คาร์บอเนตไลต์ของเกลือเพิ่มขึ้น นอกจากนี้ยังพบความสัมพันธ์ที่ดีระหว่างความเร็วคลื่นและสมบัติความหนืดพลาสติกของเกลือ การค้นพบนี้สามารถใช้ในการประเมินสมบัติเชิงกลและการไหลของเกลือจากการวัดความเร็วคลื่นอัลตราโซนิก

NISACHON PHONGKLAHAN : CORRELATIONS BETWEEN
MECHANICAL AND TIME-DEPENDENT PROPERTIES AND
ULTRASONIC PULSE VELOCITIES OF ROCK SALT. THESIS

ADVISOR : PROF. KITTITEP FUENKAJORN, Ph.D., P.E., 78 PP.

P-WAVE VELOCITY/ULTRASONIC TEST/DYNAMIC ELASTIC MODULUS/
MAHA SARAKHAM FORMATION

The objective of this study is to correlate the ultrasonic pulse velocities with the physical and mechanical properties, and mineral compositions of Maha Sarakham rock salt specimens under various carnallite and anhydrite contents. The ultrasonic pulse velocity measurements performed using OYO Sonic Viewer 170 (Model 5338). The testing includes: 1) ultrasonic pulse velocity measurements to determine dynamic properties, 2) uniaxial compression test to determine static mechanical properties, 3) uniaxial creep tests to determine salt rheological properties, and 4) X-ray diffraction analysis to identify mineral compositions of rock salt. The results indicate that density do affect the wave velocities. The results show that P-wave and S-wave velocities increases with increasing densities, mechanical and creep properties, and anhydrite contents, but decreases with increasing Poisson's ratio and carnallite contents of the salt. Good relationship is also found between the wave velocities and the visco-plastic property of the salt. The findings can be used to estimate the mechanical and rheological properties of the salt from the pulse velocity measurements.

School of Geotechnology

Academic Year 2020

Student's Signature นิสัชกร พงษ์ศักดิ์หาญ

Advisor's Signature ค. ฟูเณจอร์น

ACKNOWLEDGEMENTS

I wish to acknowledge the funding support from Suranaree University of Technology (SUT).

I would like to express thanks to Prof. Dr. Kittitep Fuenkajorn, thesis advisor, who gave a critical review. I appreciate his encouragement, suggestions, and comments during the research period. I would like to express thanks to Assoc. Prof. Dr. Pornkasem Jongpradist, Asst. Prof. Dr. Akkhapun Wannakomol and Dr. Thanittha Thongprapha for their valuable suggestions and comments on my research works as thesis committee members. Grateful thanks are given to all staffs of Geomechanics Research Unit, Institute of Engineering who supported my work.

Finally, I most gratefully acknowledge my parents and friends for all their supported throughout the period of this study.

Nisachon Phongklahan

มหาวิทยาลัยเทคโนโลยีสุรนารี

TABLE OF CONTENTS

	Page
ABSTRACT (THAI)	I
ABSTRACT (ENGLISH)	II
ACKNOWLEDGEMENTS	III
TABLE OF CONTENTS	IV
LIST OF TABLES	VIII
LIST OF FIGURES	IX
SYMBOLS AND ABBRIVIATIONS	XIII
CHAPTER	
I INTRODUCTION	1
1.1 Background and Rationale.....	1
1.2 Research Objectives.....	1
1.3 Scope and Limitations.....	2
1.4 Research Methodology.....	2
1.4.1 Literature Review.....	3
1.4.2 Sample Preparation.....	3
1.4.3 Ultrasonic Pulse Velocity (UPV) Measurement.....	4
1.4.4 Uniaxial Compression Test.....	4
1.4.5 Uniaxial Creep Test.....	4
1.4.6 X-ray Diffraction Analysis.....	4

TABLE OF CONTENTS (Continued)

	Page
1.4.7 Analysis.....	5
1.4.8 Discussions and Conclusions.....	5
1.4.9 Thesis Writing.....	5
1.5 Thesis Contents.....	5
II LITERATURE REVIEW.....	7
2.1 Introduction.....	7
2.2 Pulse Velocity of Rocks.....	7
2.3 Wave Velocity of Rock Salt.....	15
2.4 Mechanical Properties of Maha Sarakham Salt.....	18
2.5 Mineral Compositions of Rock Salt.....	20
III SAMPLE PREPARATION	22
3.1 Introduction.....	22
3.2 Sample Preparation.....	22
IV LABORATORY TESTS METHOD AND RESULTS.....	28
4.1 Introduction.....	28
4.2 Specimen.....	28
4.2.1 Density Measurements.....	28
4.2.2 Density Results.....	29
4.3 Ultrasonic Pulse Velocity (UPV).....	29
4.3.1 Ultrasonic Pulse Velocity (UPV) Measurement Method.....	29

TABLE OF CONTENTS (Continued)

	Page
4.3.2 Ultrasonic Pulse Velocity (UPV) Results.....	30
4.4 Mechanical Test.....	33
4.4.1 Uniaxial Compression Testing Method.....	33
4.4.2 Uniaxial Compression Results	35
4.5 Creep Test.....	38
4.5.1 Uniaxial Creep Test Method.....	38
4.5.2 Creep Property Results.....	39
4.6 Mineral Compositions.....	41
4.6.1 X-ray Diffraction (XRD) Analysis.....	41
4.6.2 X-ray Diffraction (XRD) Results.....	41
V DEVELOPMENT OF MATHEMATICAL	
RELATIONSHIPS	45
5.1 Introduction.....	45
5.2 Relationship between Pulse Velocity and Density.....	45
5.3 Relationship between Dynamic Properties and Density.....	46
5.4 Relationship between Mechanical Properties and	
Densities.....	50
5.5 Relationship between Mechanical and Dynamic	
Properties.....	52
5.6 Calibration of Creep Parameters.....	54

TABLE OF CONTENTS (Continued)

	Page
5.7 Correlations between Creep Parameters and Dynamic Properties.....	57
5.8 Effect of Inclusions.....	60
VI DISCUSSIONS AND CONCLUSIONS	69
6.1 Discussions.....	69
6.2 Conclusions.....	71
6.3 Recommendations for Future Studies.....	72
REFERENCES	73
BIOGRAPHY	78



LIST OF TABLES

Table	Page
2.1	Pulse velocity data from various researchers..... 13
2.2	Pulse velocity data of rock salt.....17
2.3	Material property parameters used in the FLAC of Maha Sarakham salt studied by Luangthip et al. (2017)19
2.4	Mineral compositions on pulse velocity.....21
3.1	Dimensions and densities of rock salt prepared for uniaxial compression testing.....24
3.2	Dimension and density of rock salt prepared for uniaxial creep testing.....26
4.1	Ultrasonic pulse velocities and dynamic parameter of salt specimens.....31
4.2	Results from the uniaxial compression test.....37
4.3	Result of X-ray diffraction analyses of uniaxial compression test.....42
4.4	Result of X-ray diffraction analyses of uniaxial creep test.....44
5.1	Results from calibration of uniaxial creep test data against Burgers model.....55

LIST OF FIGURES

Figure	Page
1.1	Research methodology.....3
2.1	Uniaxial compressive strength as a function of P-wave velocity of (a) NLC sandstones and (b) SCCL sandstones 8
2.2	Relationship between UPV and granite compressive strength, Young modulus and dry density9
2.3	Relationship between uniaxial compressive strength and static young's modulus versus dynamic young's modulus10
2.4	P- and S-waves velocity versus density of dry rock samples11
2.5	P-wave velocity and S-wave velocity versus uniaxial compressive strength of rock samples12
2.6	P-wave velocity-density relationship for different lithologies15
2.7	Cross-plot of shear and compressional velocities17
2.8	Burgers parameters as a function of Lode parameter (μ)20
3.1	Stratigraphy and location of Maha Sarakham formation22
3.2	Some specimens for ultrasonic pulse velocity (UPV) measurements.....23
3.3	Rock salt powder for X-ray diffraction (XRD) analysis27
4.1	Direct method of ultrasonic pulse velocity measurements using by OYO Sonic viewer 170 Model 5338.....29
4.2	Uniaxial compression test device.....34

LIST OF FIGURES (Continued)

Figure	Page
4.3	Stress-stain curves from uniaxial compression tests of salt specimens with $C\% = 11-16\%$35
4.4	Stress-stain curves from uniaxial compression tests of salt specimens with $C\% = 3-10\%$36
4.5	Stress-stain curves from uniaxial compression tests of salt specimens with $A\% = 4-8\%$36
4.6	Stress-stain curves from uniaxial compression tests of salt specimens with $A\% = 10-27\%$37
4.7	Uniaxial creep test device.....39
4.8	Octahedral shear strain as a function of $C\%$. Solid lines are test results. Dash lines are curve fits with Burgers model.....40
4.9	Octahedral shear strain as a function of $A\%$. Solid lines are test results. Dash lines are curve fits with Burgers model.....40
4.10	X-ray diffraction Bruker, D2 Phaser (The Center for Scientific and Technology Equipment, Suranaree University of Technology) 41
5.1	Relationship between P- and S-wave velocities and density.....46
5.2	Relationship between P-wave and S-wave velocities.....47
5.3	Relationship between dynamic elastic modulus and density.....47
5.4	Relationship between dynamic Poisson's ratio and density.....49
5.5	Relationship between dynamic Young's modulus and P- and S-wave velocities.....49

LIST OF FIGURES (Continued)

Figure	Page
5.6 Relationship between dynamic Poisson's ratio and P- and S-wave velocities.....	50
5.7 Relationship between uniaxial compressive strength and density.....	51
5.8 Relationship between static elastic modulus and density.....	51
5.9 Relationship between static Poisson's ratio and density.....	53
5.10 Relationship between uniaxial compressive strength and P- and S-wave velocities.....	53
5.11 Relationship between static elastic modulus and dynamic elastic modulus.....	54
5.12 Static Poisson's ratio as a function of dynamic Poisson's ratio.....	56
5.13 Relationship between the elastic modulus and P- and S-wave velocities.....	57
5.14 Spring constant in visco-elastic phase as a function of P- and S-wave velocities.....	59
5.15 Relationship between the visco-plastic coefficient and P- and S-wave velocities.....	59
5.16 Relationship between the visco-elastic viscosity and P- and S-wave velocities.....	60
5.17 Salt specimen density as a function of carnallite and anhydrite contents.....	61
5.18 P-wave and S-wave velocities as a function of carnallite and anhydrite contents.....	62

LIST OF FIGURES (Continued)

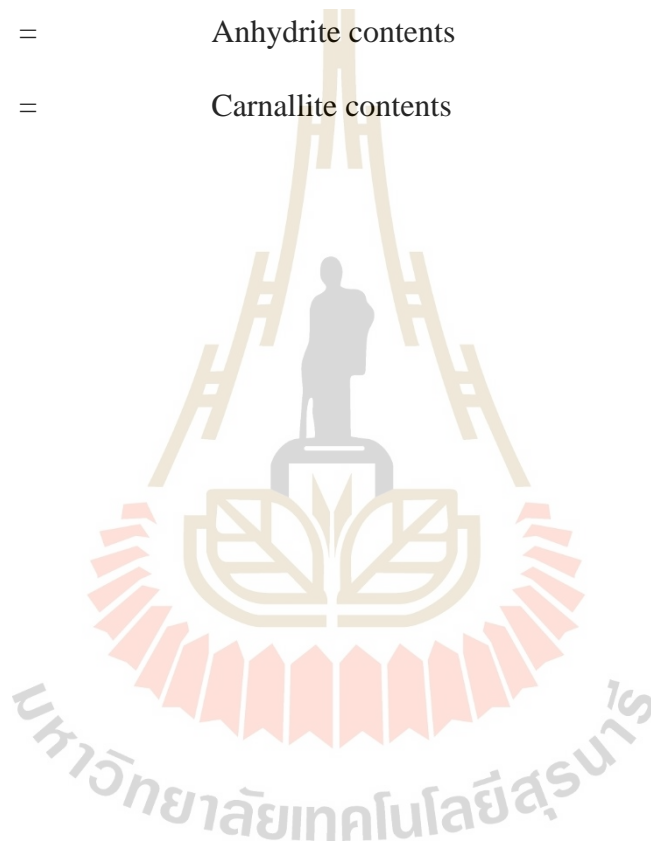
Figure	Page
5.19 Dynamic Young's modulus as a function of carnallite and anhydrite contents.....	63
5.20 Dynamic Poisson's ratio as a function of carnallite and anhydrite contents.....	63
5.21 Uniaxial compressive strength as a function of carnallite and anhydrite contents.....	64
5.22 Static elastic modulus as a function of carnallite and anhydrite contents.....	65
5.23 Static Poisson's ratio as a function of carnallite and anhydrite contents.....	65
5.24 The elastic modulus as a function of carnallite and anhydrite contents.....	66
5.25 The spring constant in visco-elastic phase as a function of carnallite and anhydrite contents.....	67
5.26 The visco-plastic coefficient as a function of carnallite and anhydrite contents.....	67
5.27 The visco-elastic viscosity as a function of carnallite and anhydrite contents.....	68

SYMBOLS AND ABBREVIATIONS

ρ	=	Density
m	=	Mass
V	=	Volume
V_p	=	P-waves velocity
V_s	=	S-waves velocity
E_d	=	Dynamic elastic modulus
E_s	=	Static elastic modulus
ν_d	=	Dynamic Poisson's ratio
σ_c	=	Uniaxial compressive strength
σ_1	=	Axial stress
σ_2	=	Intermediate principal stress
μ	=	Lode parameter
P	=	Failure load
A	=	Initial cross-sectional area
E	=	Static elastic modulus
ν	=	Poisson's ratio
γ_{oct}	=	Octahedral shear strain
ϵ_1	=	Axial strain
ϵ_2	=	Intermediate strains
ϵ_3	=	Lateral strain

SYMBOLS AND ABBREVIATIONS (Continued)

E_1	=	The elastic modulus
E_2	=	The spring constant in visco-elastic phase
η_1	=	Visco-plastic viscosity
η_2	=	Visco-elastic viscosity
$A\%$	=	Anhydrite contents
$C\%$	=	Carnallite contents



CHAPER I

INTRODUCTION

1.1 Background and Rationale

Ultrasonic velocity measurement is a non-destructive and indirect testing method which is used to determine physical and mechanical properties of rocks. This technique has been used to study the properties of rock salt in many countries (Gardner et al., 1974; Serra, 1990; Jones and Davison, 2014; Zong et al., 2015; Teixeira and Lupinacci, 2019). Several investigators (Fuenkajorn and Phueakphum, 2010; Wilalakand Fuenkajorn, 2016; Luangthip et al., 2017; Phatthaisong et al., 2018) have determine the mechanical and rheological properties of rock salt to improve an understanding of the behavior of Maha Sarakham salt, northeast of Thailand. The relationships between dynamic mechanical properties obtained from the pulse velocity test and static mechanical properties have however, rarely been studied, especially under varying inclusion (carnallite and anhydrite) contents.

1.2 Research Objective

The objective of this study is to determine the correlations between ultrasonic pulse velocity, physical and mechanical properties, and mineral compositions of Maha Sarakham rock salt. The ultrasonic test (pulse velocity P and S-waves) conducted on salt specimens with varying inclusion contents. The mechanical properties obtained from uniaxial compression and uniaxial creep tests. The mineral compositions analyzed by X-ray diffraction. The influence of inclusions on physical and mechanical properties

of salt determined. The comparison between dynamic and static mechanical properties performed.

1.3 Scope and Limitations

The scope and limitations of the research include as follows.

- 1) Laboratory test conducted on rock salt specimens obtained from the Lower Salt member of the Maha Sarakham formation.
- 2) The salt specimens prepared to obtain cylindrical specimens with nominal diameters of 62 mm. The length-to-diameter ratios (L/D) are 2.0.
- 3) Ultrasonic test method and calculation follow the ASTM D2845-08 standard practice.
- 4) Uniaxial compression test procedures conducted in accordance with the ASTM D7012-14 standard practice.
- 5) Uniaxial creep tests performed under constant axial stress of 10 MPa for 10 days. The testing procedures follow the ASTM D7070-08 standard practice.
- 6) Mineral compositions analyzed using X-ray diffraction method (XRD).
- 7) The research findings published in conference paper or journal.
- 8) Bedding planes are normal to the core axis.

1.4 Research Methodology

The research methodology (Figure 1.1) comprises 9 steps; including literature review, sample collection and preparation, pulse velocity measurement, uniaxial compression test, uniaxial creep test, X-ray diffractometer, data analysis, discussions and conclusions and thesis writing.

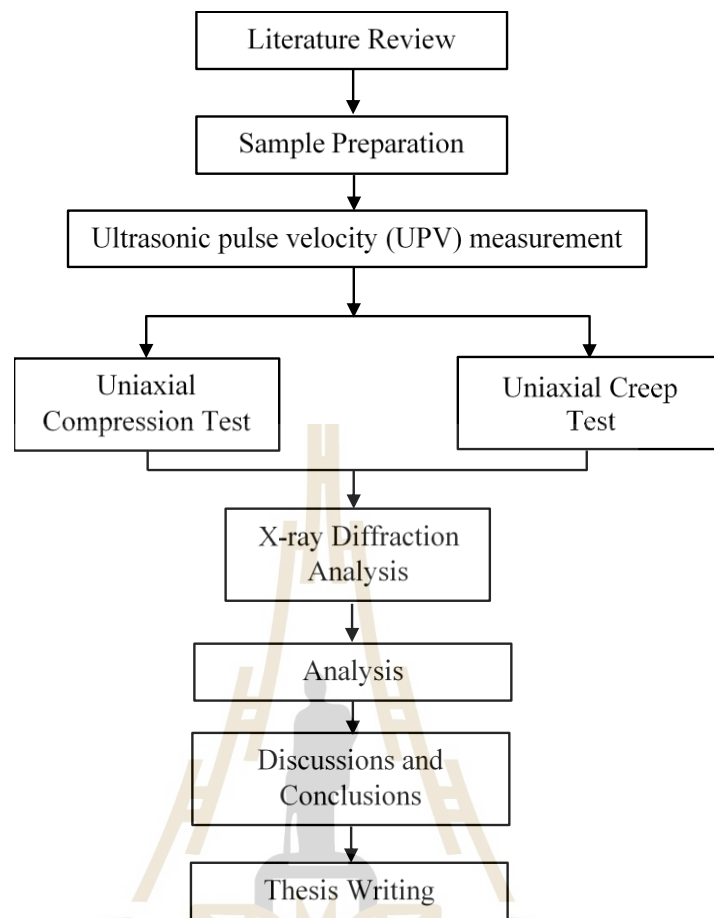


Figure 1.1 Research methodology.

1.4.1 Literature Reviews

Literature reviews carried out to study the experimental researches on the pulse velocity, uniaxial compression test, uniaxial creep test and X-ray diffractometer. The sources of information are from textbooks, journals, and conference papers. A summary of the literature review given in the thesis.

1.4.2 Sample Preparation

The rock salt obtained from the Lower Salt member of Maha Sarakham formation, northeastern of Thailand. Sample preparation carried out in laboratory at Suranaree University of Technology. The specimens prepared to obtain cylinder with

nominal a length-to-diameter ratios (L/D) of 2.0 to 2.5, and a diameter should not less than 47 mm (ASTM D7012-14).

1.4.3 Ultrasonic Pulse Velocity (UPV) Measurement

A total rock salt of 73 specimens measured P- and S-waves velocity using by OYO Sonic Viewer 170 (Model 5338) before they subjected to the mechanical testing. The test method and calculation follow the ASTM D2845-08 standard practice. The wave velocity can be used to calculate dynamic elastic modulus and Poisson's ratio.

1.4.4 Uniaxial Compression Test

The uniaxial compression properties determined following the ASTM D7012-14 standard practice. The axial and lateral displacements monitored and recorded. Total 51 specimens tested. The results used to determine static, elastic modulus and Poisson's ratio.

1.4.5 Uniaxial Creep Test

Uniaxial creep tests conducted following ASTM D7070-08 standard practice. A total of 22 specimens performed under constant axial stress of 10 MPa for up to 10 days. The dial gages installed to measure the axial and lateral deformations. The time-related displacements are recorded and analyzed. The results are used to calibrate the elastic, visco-plastic and visco-elastic parameters of rock salt by using SPSS statistical software (Wendai, 2000).

1.4.6 X-ray Diffraction Analysis

The XRD analysis is performed on finely ground rock salt powder with particle sizes less than 0.25 mm pressed into coherent pellets. The analysis is performed after uniaxial compression test and uniaxial creep test. The X-ray diffraction (Bruker, D2 Phaser) used. The results can be used to identify the effect of inclusions (impure

rock salt) among the salt specimens on changing to mineral compositions which may affect rock salt stability.

1.4.7 Analysis

The results obtained from the pulse velocity test, uniaxial compression test, uniaxial creep test and XRD analyses of rock salt analyzed to determine the relationship between physical, mechanical and mineral compositions parameters with the pulse velocity for use to predict the properties of rock salt.

1.4.8 Discussions and Conclusions

Discussions made to describe the reliability and adequacy of the test data. Comparison of the results obtained here with those obtained elsewhere made in terms of similarity and discrepancy. Explanations on these issues offered. Conclusions from the research study drawn. The research or findings published in the conference proceedings or inter journals.

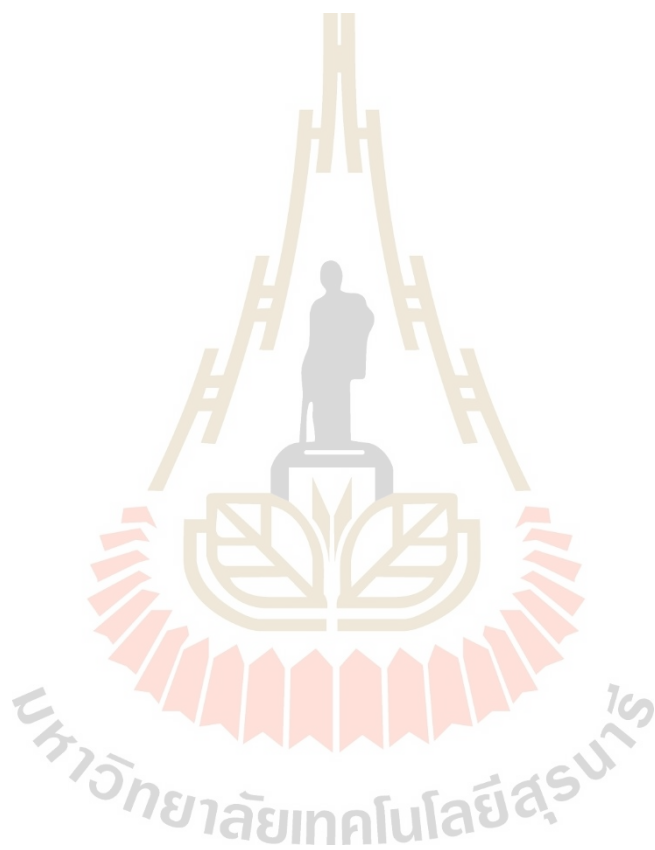
1.4.9 Thesis Writing

All research activities and results documented and complied in the thesis. This study can be applied to determination relationship pulse velocity and uniaxial compression tests, uniaxial creep test and mineral composition. The findings published in the conference proceedings or journals.

1.5 Thesis Contents

Chapter I describes the background of problems and significance of the study. The research objectives, methodology, scope and limitations are identified. Chapter II summarizes the results of the literature review. Chapter III describes the sample preparations. Chapter IV describes the laboratory testing. Chapter V describes dynamic and mechanical properties and XRD analyses of rock salt. Chapter VI discusses and

concludes the research results and provides recommendations for future research studies.



CHAPTER II

LITERATURE REVIEW

2.1 Introduction

This chapter summarizes the results of literature review carried out to improve an understanding of the relationship between wave velocity (P-wave and S-wave velocity) with physical and mechanical properties and mineral compositions of rocks. The topics reviewed here include wave velocity of rocks in the laboratory and in the field, and factors controlling the wave velocities of rocks.

2.2 Pulse Velocity of Rocks

Wave is one of the tools used to explore physical characteristics of materials. Geophysical surveys use the properties of seismic waves. For the study of the internal structure of the world, characteristics of rock masses in the crust and the phenomena on earth, such as earthquakes. Smaller scale surveys are performed on mineral areas or project area for foundations on rock. Ultrasonic waves can be created from devices convert energy into transducers (a transmitter and a receiver). The waves can move through both solid and liquid media. Ultrasonic movement is applied in engineering and geotechnology such as inspection of concrete, metal, ceramic, rocks. It is a way to measure the pulse velocity passing through the sample and pulse velocity which can be calculated for mechanical properties by not-destroying sample. The test equipment is not very large, it can be used easily in both laboratory and field. It has been developed for use in geotechnical engineering, geotechnical and mining and inspection of rock.

properties from specimens (Wannakao et al., 2007; 2009)

Song et al. (2004) study ultrasonic measurements of compressional and shear wave velocities on cylindrical specimens prepared across and along the foliations. Under hydrostatic pressure up to 70 MPa. They determined the complete set of dynamic moduli of foliated metamorphic rocks with two assumptions; transverse isotropy due to the foliation and ellipsoidal seismic energy propagation from a point source. The calculated elastic moduli referring to different directions could be valuable for the design of engineering structures in rock mass.

Chary et al. (2006) state that ultrasonic pulse velocity (UPV) can be used to determine the properties of rocks. They have performed UPV measurements and uniaxial strength (UCS) tests on sandstone samples. The engineering properties such as brittleness, hardness, fracture toughness and drill ability index of rocks have been obtained. They found that there is a fairly good correlation between UPV and UCS, UPV and the mechanical properties of sandstones. The uniaxial strength increases with

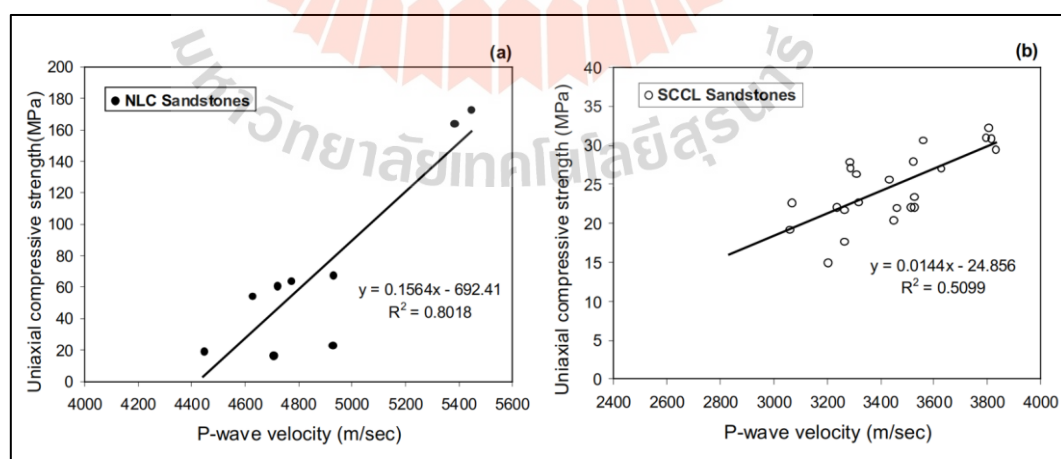


Figure 2.1 Uniaxial compressive strength as a function of P-wave velocity of

(a) NLC sandstones and (b) SCCL sandstones (Chary et al., 2006).

increasing wave velocity because ultrasonic pulse speed passes well (Figure 2.1). The test results agree well with those obtained by Vasconcelos et al. (2008), Moradian and Behnia (2009), Altindag (2012), Khandelwal (2013), Jaroenklang et al. (2017), Saroglou and Kallimogiannis (2017), Aldeeky and Al Hattamleh (2018), Chawre (2018), and Abdullah et al. (2019).

Vasconcelos et al. (2008) state that elastic properties are useful for the performance of built structures and UPV can be used in the estimation of the strength. Figure 2.2 shows each type of stone that has different uniaxial compressive strength, Young's modulus and dry density. As these properties increase, the wave also increases.

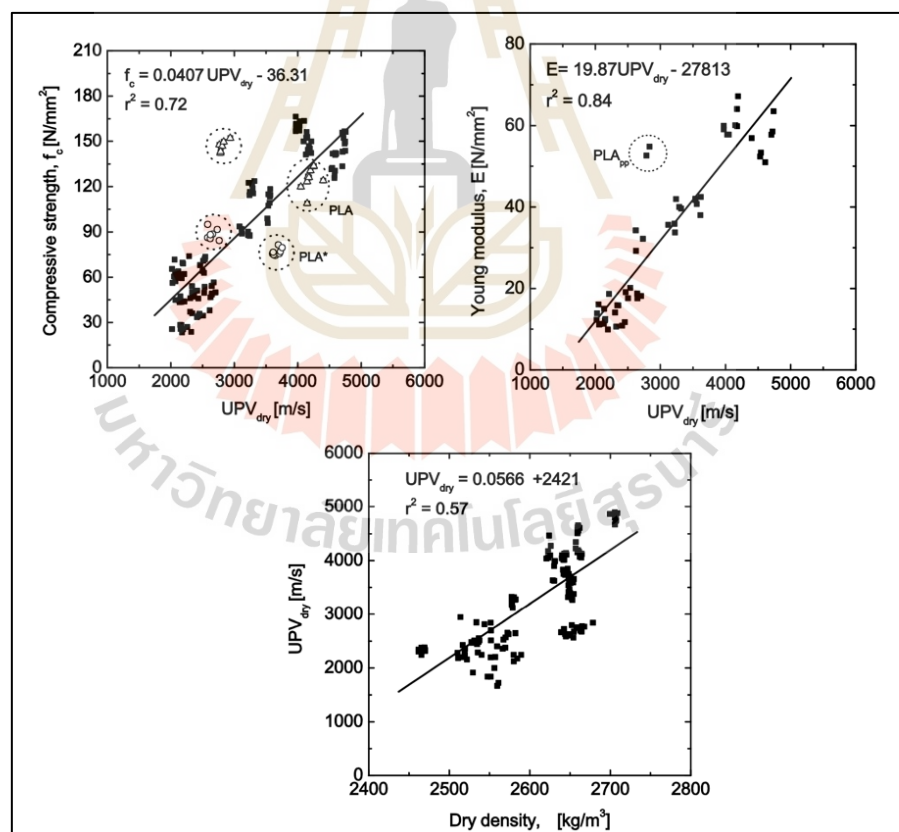


Figure 2.2 Relationship between UPV and granite compressive strength,

Young modulus and dry density (Vasconcelos et al., 2008).

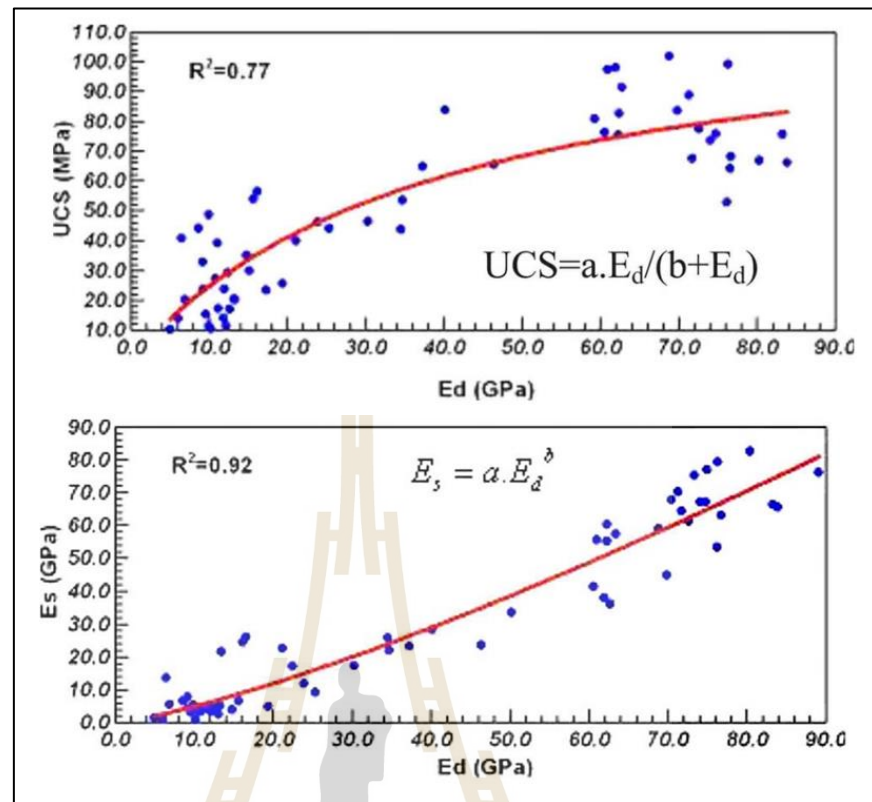


Figure 2.3 Relationship between uniaxial compressive strength and static young's modulus versus dynamic young's modulus (Moradian and Behnia, 2009).

Moradian and Behnia (2009) study uniaxial compressive strength and static Young's modulus (ES) of intact rocks. By using the ultrasonic test, one can indirectly predict these parameters. Figure 2.3 shows that the strength and static Young's modulus increase with increasing dynamic Young's modulus.

Altindag (2012) studies relationships between P-wave velocity and physical-mechanical properties by simple regression analysis. Khandelwal (2013) studies relationships between the different physico-mechanical properties of various rock types with the P-wave velocity. Saroglou and Kallimogiannis (2017) study the effect of fracturing degree on P- and S-wave velocities in rock. Aldeeky and Al Hattamleh

(2018) study mechanical properties (dry density, porosity, uniaxial compressive strength, and Brazilian tensile strength) of basalt. The ultrasonic pulse velocity (UPV) test was used to determine the engineering properties.

Chawre (2018) examines some properties of quartz-mica schist (QMS) rocks in a cost-effective manner by establishing correlations between non-destructive and destructive tests. Figure 2.4 shows that as the density increases, the P-wave and S-wave velocity will increase. Figure 2.5 shows that as the uniaxial strength increases, the P- and S-wave velocities will increase.

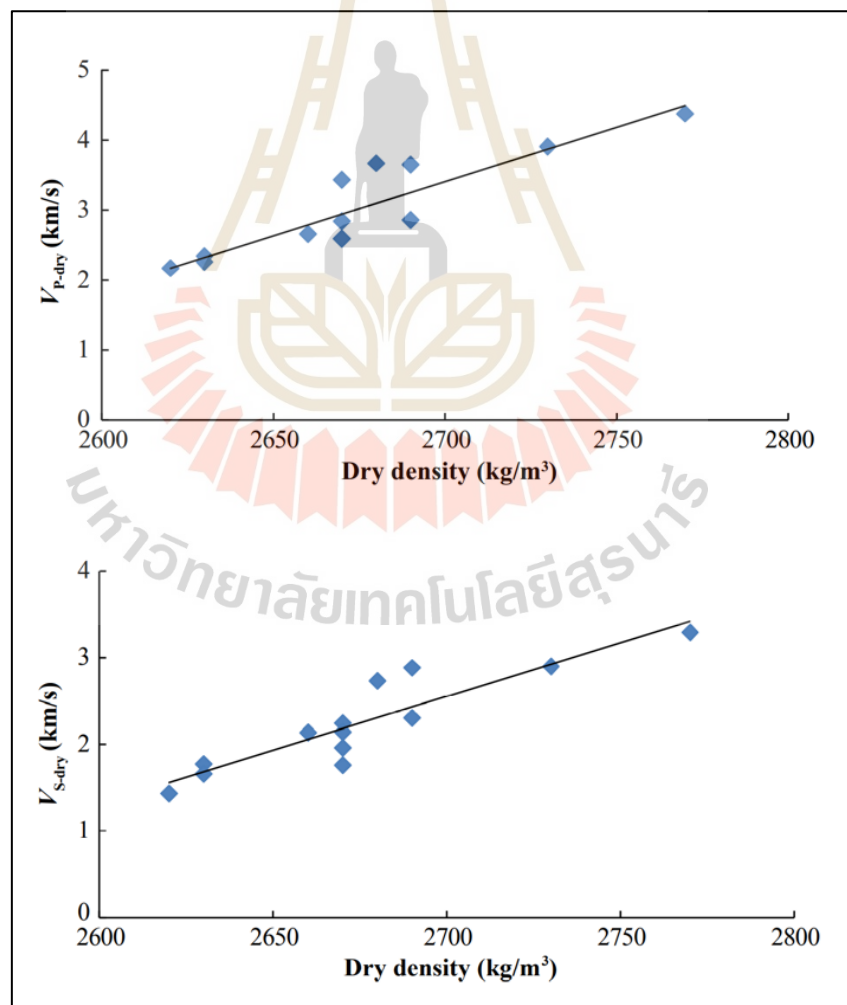


Figure 2.4 P- and S-waves velocity versus density of dry rock samples (Chawre, 2018).

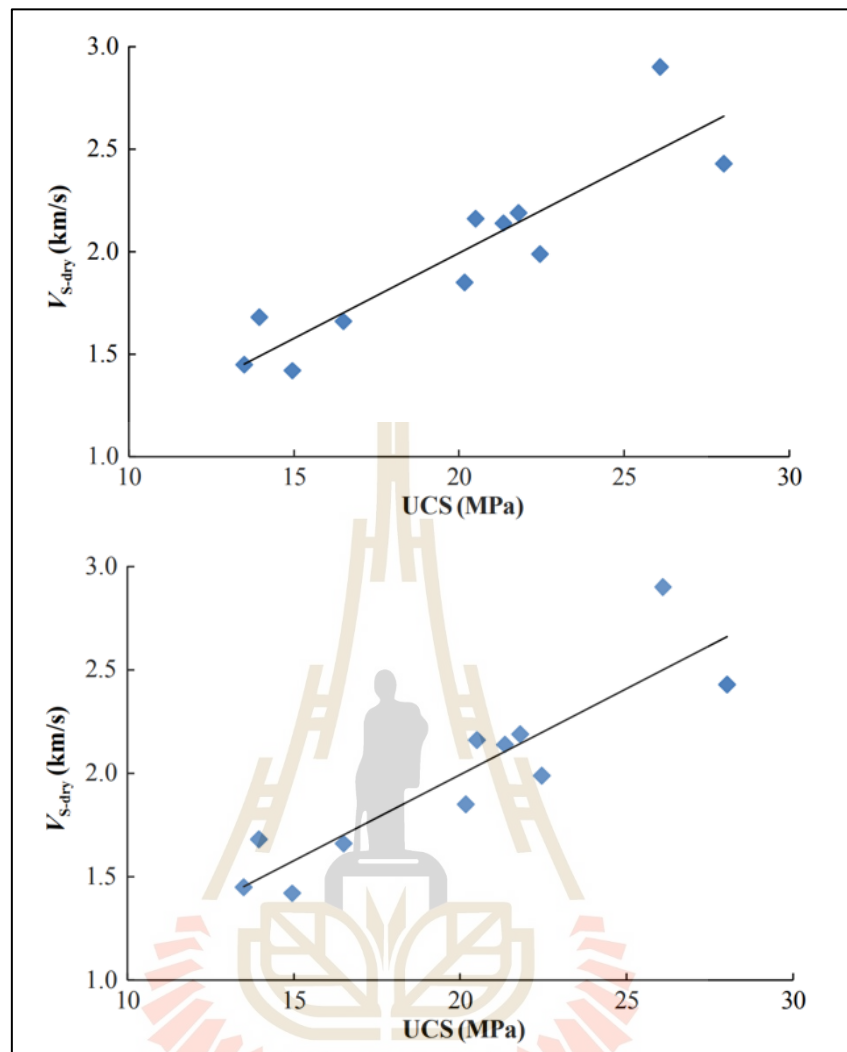


Figure 2.5 P-wave velocity and S-wave velocity versus uniaxial compressive strength of rock samples (Chawre, 2018).

Abdullah et al. (2019) develop empirical models based on laboratory testing using seismic velocity parameters and deformation properties. The relationship between elastic properties and seismic velocity of tropical sedimentary rocks can be used for construction of foundation building. Young's modulus, shear modulus and bulk modulus can be determined by conducting UCS test with deformation measurement. The relationship between P-wave velocity and elastic properties

parameters. The result of allowable soil bearing pressure can be used for design foundation building. The laboratory analysis of samples is used to predict P-wave velocity.

Ultrasonic techniques are used to testing various types of rocks. The results show the range of pulse velocity (P-wave, V_p and S-wave, V_s), as shown in Table 2.1. For homogeneous rock samples, the waves move faster (Leucci and De Giorgi, 2006). The values of V_p and V_s are highest, but if there is the fracture in the specimen, it will cause the waves to move slowly.

Table 2.1 Pulse velocity data from various researchers.

Rock Type		ρ (g/cm ³)	V_p (km/s)	V_s (km/s)	References
Serpentine		2.64-2.74	5.252-5.970	2.823-3.406	Song et al. (2004)
Talc		2.81	5.097-5.180	2.961-2.988	
Amphibole schist		3.04-3.09	6.250-6.448	3.546-3.621	
Biotite schist		2.70-2.85	5.132-5.419	2.932-3.172	
Granite gneiss		2.72-2.75	4.313-5.263	2.714-3.112	
Sandstones	NLC	-	4.669	-	Chary et al. (2006)
	SCCL	-	3.345	-	
Granite		-	1.899-4.804	-	Vasconcelos et al. (2008)
Limestone		2.10-2.92	1.826-6.539	0.900-3.420	Moradian and Behnia (2009)
Sandstone		2.22-2.44	1.840-2.674	1.104-1.532	
Marlstone		2.04-2.32	2.451-2.948	1.314-2.044	
Sandstone		-	2.385-5.330	-	Altindag (2012)
Limestone		-	2.200-6.750	-	
Marl		-	1.000-3.400	-	
Mudrock-Shale		-	2.548	-	
Travertine		-	4.500	-	
Dolomite		-	6.300	-	

Table 2.1 Pulse velocity data from various researchers (cont.).

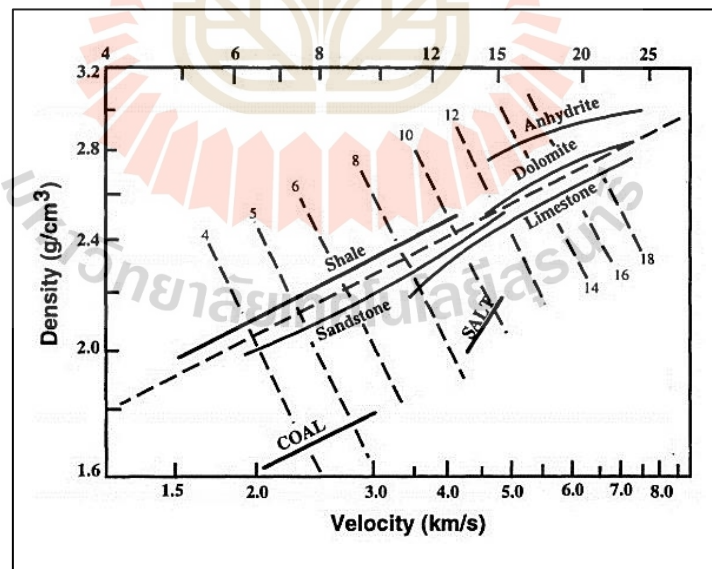
Rock Type		ρ (g/cm ³)	Vp (km/s)	Vs (km/s)	References
Siltstone		-	4.950	-	Altindag (2012)
Slate		-	4.743-5.046	-	
Serpentine		2.43-2.66	2.470	1.396	Kurtulus et al. (2012)
Kd (serpentine, gabbro, peridotite etc.)	across foliation	2.43-2.66	4.110-5.289	-	Kurtulus et al. (2012)
	along foliation		4.419-5.633	-	
Quartz		2.74	4.657	-	Khandelwal (2013)
Granite		2.67	4.350	-	
Dolerite		2.58	3.283	-	
Sandstone		2.16-2.36	2.146-2.384	-	
Limestone		2.33-2.37	3.016-3.108	-	
Shale		2.07	1.682	-	
Kota stone		2.58	4.375	-	
Marble		2.28-2.56	2.370-3.239	-	
Travertine		-	4.87±0.05	2.90±0.06	Jaroenklang et al. (2017)
Marble		-	5.22±0.15	3.10±0.09	
Granite		2.61	4.927	3.173	Saroglou and Kallimogiannis (2017)
Basalt		2.65	5.050	-	Aldeeky and Al Hattamleh (2018)

Table 2.1 Pulse velocity data from various researchers (cont.).

Rock Type	ρ (g/cm ³)	V _p (km/s)	V _s (km/s)	References
Quartz-mica schist	2.62-2.78	2.300-4.980	1.660-3.860	Chawre (2018)
Sandstone	2.16-3.04	0.780-5.210	0.374-3.413	Abdullah et al. (2019)

2.3 Wave Velocity of Rock Salt

Gardner et al. (1974) state that salt is a special type of rock. It has high velocity (4.5 to 5.5 km/s) and low density (2000 to 2200 kg/m³). Salt may be changed from elastic to anelastic rock at lower temperature and pressure, compared with other sedimentary rocks. Each type of stone has different density (Figure 2.6). As the density increases, the speed also increases as high-speed waves pass well.

**Figure 2.6** P-wave velocity-density relationship for different lithologies

(after Gardner et al., 1974).

Popp et al. (2001) study combined gas permeability and P and S wave velocity measurement were carried out on rock salt sample from the Gorleben salt dome and the Morslen salt mine under hydrostatic and triaxial loading conditions, mostly at room temperature. Permeabilities in the as-received samples vary between 10^{-16} and 2×10^{-20} m². This suggests that the evolution of permeability is not only a function of dilatancy but also of microcrack linkage. Importantly, the anisotropic crack array within the samples causes a strong directional dependence of permeability.

Zong et al. (2015) study the densities and elastic properties of rock salt from benchtop ultrasonic measurements, log data analysis in the Gulf Coast regions, and seismic survey designs, acquisition and interpretations over salt domes. They found that P-wave velocity V_p (km/s) increases with depth D (km) of the salt as: $V_p = 4.41 + 0.0104 \cdot D$, with the average standard deviation of 0.10 km/s. The salt electron density readings concentrate at 2.06 ± 0.1 g/cm³.

Teixeira and Lupinacci (2019) propose an approach to evaluate the internal structures of salt bodies in the Santos Basin, offshore Brazil, using well and 3D seismic data. They perform seismic inversion to generate spatial distribution of acoustic impedance. They derive compressional and shear velocities, density, Young's modulus and Poisson's ratio volumes by applying the empirical equations to the acoustic impedance. The blind well points out that, through this workflow, the seismic data can predict the elastic properties of salt formation in undrilled portions. Figure 2.7 illustrates that P-velocity and S-velocity will increase accordingly.

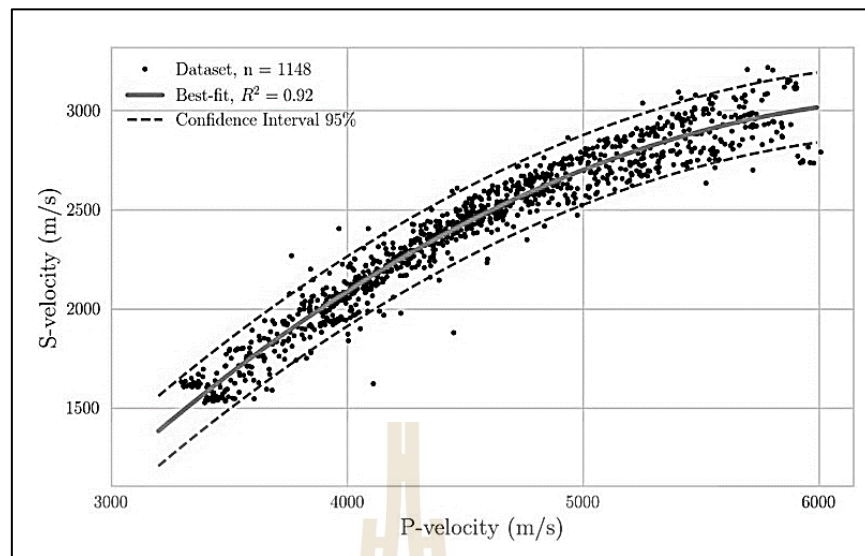


Figure 2.7 Cross-plot of shear and compressional velocities (Teixeira & Lupinacci, 2019).

The results show the range of pulse velocity (P-wave, V_p and S-wave, V_s), as shown in Table 2.2 shows data studied rock salt by many researchers (Serra, 1990; Popp et al., 2001; Jones and Davison, 2014; Zong et al., 2015).

Table 2.2 Pulse velocity data of rock salt.

Rock Type		V_p (km/s)	V_s (km/s)		References
Halite		4.57	-		Serra (1990)
Rock salt		4.28-4.58	2.52-2.66		Popp et al. (2001)
Halite		4.50	-		Jones and Davison (2014)
Goderich Salt Mine, Ontario, Canada	Direction symmetric axis	4.75	2.46		Zong et al. (2015)
	Halfway between two symmetric axes	4.44	2.92	2.47	
Bayou Salt Dome, Louisiana		4.45 ± 0.02	2.59 ± 0.03		

Table 2.2 Pulse velocity data of rock salt (cont.).

Rock Type	Vp (km/s)	Vs (km/s)	References
Hock Salt Mine, Houston, TX	4.64±0.09	2.70±0.05	Zong et al. (2015)
Zipaquira´	4.19±0.18	2.46±0.12	
Salt Layer	4.50	2.25	

2.4 Mechanical Properties of Maha Sarakham Salt

Fuenkajorn and Phueakphum (2010) determine uniaxial and triaxial compressions and Brazilian tension strength of Maha Sarakham salt. The elastic modulus of the salt is 25.2±1.9 GPa. The Poisson's ratio is 0.37±0.11. The uniaxial compressive and Brazilian tensile strengths are 34.7±2.2 MPa and 1.5±0.4 MPa. The internal friction angle is calculated as 39° and the cohesion as 15 MPa.

Wilalak and Fuenkajorn (2016) determine the effects of carnallite contents on the instantaneous and time-dependent deformations of rock salt from the Maha Sarakham formation. Regression analysis is performed on the test results to calibrate the elastic, visco-elastic and visco-plastic parameters. Then, Luangthip et al. (2017) study the effects of carnallite contents on the strength, elasticity, and time-dependent parameters of rock salt specimens obtained from the Lower Member of the Maha Sarakham formation. The test results indicate that the compressive and tensile strengths and elastic moduli of the specimens exponentially decrease with increasing C%. Specimens with higher C% dilate more than those with lower C%, as evidenced by the increasing of the Poisson's ratio. The strength reduction due to the carnallite content decreases as the confining pressures increase. The elastic, visco-elastic, and visco-plastic parameters of the creep test specimens are defined as a function of C%, as shown in Table 3.

Phatthaisong et al. (2018) perform uniaxial and triaxial compression tests to assess the effects of temperature and loading rate on strength and deformability of Maha Sarakham salt. The salt strength and stiffness increase with the loading rate, and decrease with temperature. The Maha Sarakham salt properties, are shown in Table 2.3.

Table 2.3 Material property parameters used in the FLAC of Maha Sarakham salt studied by Luangthip et al. (2017).

	Parameters	Units	Lower salt
Material properties	Density	kg/m ³	1760-2110
	Bulk Modulus	GPa	3.00-12.00
	Shear Modulus	GPa	0.66-6.66
	Elastic Modulus	GPa	0.29-2.33
	Poisson's ratio	-	0.27-0.40
	Tensile strength	MPa	0.23-1.88
Creep properties	Spring constant in visco-elastic phase	GPa	0.36-2.16
	visco-plastic viscosity	GPa·day	1.04-42.30
	visco-elastic viscosity	GPa·day	0.10-1.35

Archeeploha et al. (2017) perform true triaxial creep test to determine the effects of the intermediate principal stress on the time-dependent behavior of the Maha Sarakham salt. The Burgers model indicates that the instantaneous deformation tends to be independent of s_2 . The visco-elastic and visco-plastic parameters significantly increase with s_2 . Figure 2.8 shows the Burgers parameters as a function of the Lode parameter (μ).

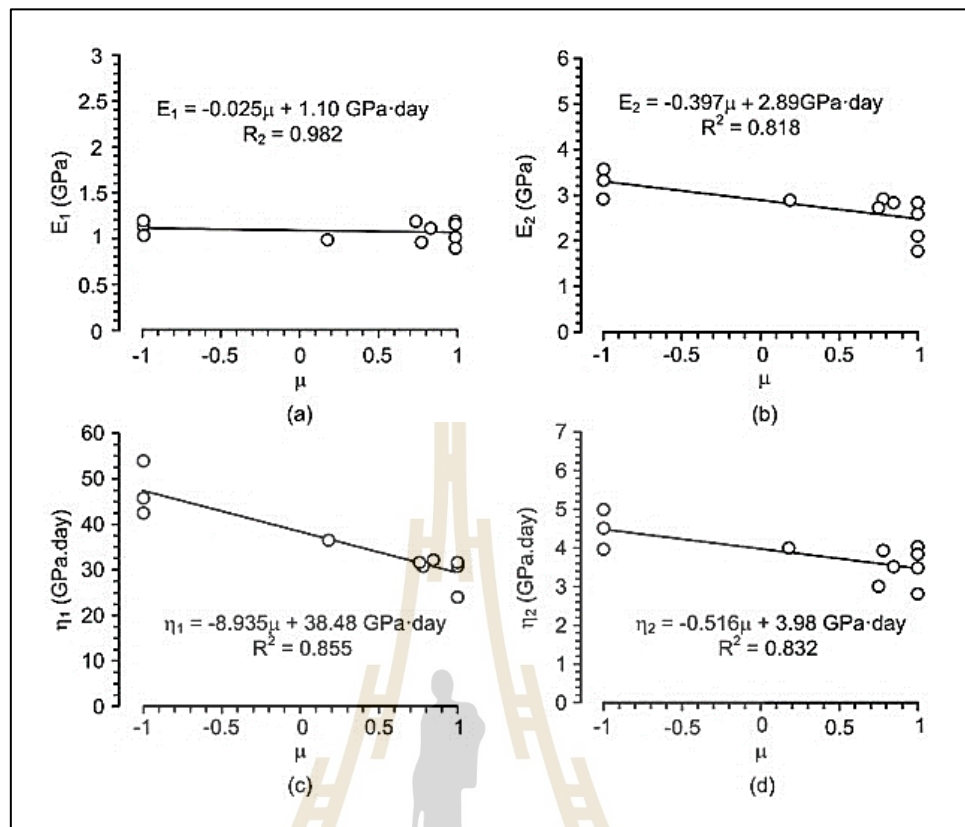


Figure 2.8 Burgers parameters as a function of Lode parameter (μ)
(Archeeploha et al., 2017).

2.5 Mineral Compositions of Rock Salt

Jones and Davison (2014) study seismic imaging of evaporite bodies which is significantly difficult due to the complex shapes of steeply dipping flanks, adjacent overburden strata, the strong acoustic impedance and velocity contrasts at the sediment-evaporite interface. When a salt model is being built, it is often assumed that the evaporite body is pure halite with a constant compressional wave speed of 4500 m/s. Almost all salt bodies contain varying amounts of gypsum ($V_p = 5700 \text{ m/s}$) or anhydrite ($V_p = 6500 \text{ m/s}$), and some bodies contain significant amounts of K-Mg-rich salts with seismic velocities as low as 3500 m/s shown in Table 2.4.

Table 2.4 Mineral compositions on pulse velocity.

Mineral	Pulse velocity (km/s)	Density (g/cm ³)	References
Tachyhydrite	3.313	1.66	Serra (1990)
Carnallite	3.908	1.56	
Sylvite	4.130	1.86	
Halite	4.570	2.03	
Anhydrite	6.096	2.95	
Halite	4.500	2.20	Jones and Davison (2014)
Gypsum	5.700	2.30	
Anhydrite	6.500	2.90	
Tachyhydrite	3.500	1.66	
Sylvite	4.110	1.99	
Carnallite	3.900	1.60	
Kieserite	-	2.55	
Langbeinite	5.860	2.82	
Polyhalite	5.300	2.79	
Dolomite	6.300	2.87	

Zong et al. (2015) perform component analysis and ultrasonic velocity measurement to determine the rock physical properties of rock salt. The components are studied from the joint analysis of X-ray powder diffraction (XRD) and the inductively coupled plasma-mass spectrometry (ICP-MS).

CHAPTER III

SAMPLE PREPARATION

3.1 Introduction

This chapter describes the sample preparation of rock salt to be used in the ultrasonic pulse velocity measurements, uniaxial compression tests, uniaxial creep tests and X-ray diffraction analysis. The rock salt is obtained from Maha Sarakham formation.

3.2 Sample Preparation

Rock samples used in this study are from Lower Salt member of Maha Sarakham formation, northeastern of Thailand (Figure 3.1).

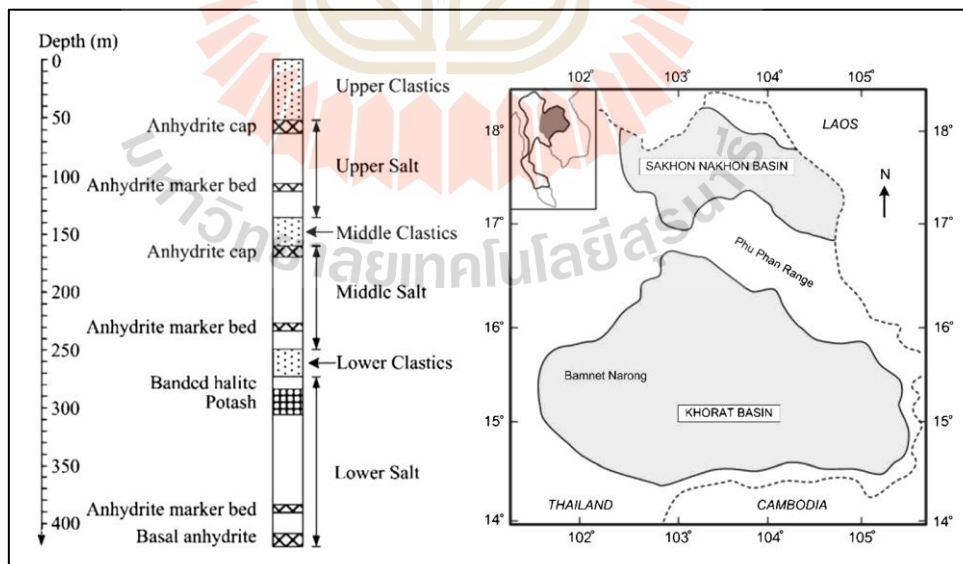


Figure 3.1 Stratigraphy and location of Maha Sarakham formation

(Luangthip et al., 2017).

The cylinder-shaped specimens with nominal size of 62 mm and 84 mm in diameters and with L/D ratio of 2.0 (Figure 3.2) are prepared. A total of seventy-three specimens is prepared to measure P- and S-waves velocities using OYO Sonic Viewer 170 (Model 5338).

Fifty-one specimens are prepared for uniaxial compression test. Table 3.1 shows dimensions and densities of the tested specimens.



Figure 3.2 Some specimens for ultrasonic pulse velocity (UPV) measurements.

Table 3.1 Dimensions and densities of rock salt prepared for uniaxial compression testing.

No.	Weight (g)	Diameter (mm)	Length (mm)	Density (g/cc)
1	757.29	63.20	115.58	2.088
2	775.74	62.90	119.04	2.096
3	839.32	63.29	126.99	2.100
4	819.85	62.50	127.20	2.100
5	835.81	62.66	128.60	2.107
6	700.34	62.60	107.60	2.114
7	838.46	63.00	127.14	2.115
8	910.47	62.67	139.31	2.118
9	743.50	62.80	113.10	2.121
10	811.41	63.20	121.80	2.123
11	772.02	62.80	117.36	2.123
12	830.95	63.49	123.59	2.123
13	778.82	63.21	116.69	2.126
14	628.86	60.82	101.74	2.127
15	786.43	62.68	119.62	2.130
16	822.79	63.46	122.07	2.130
17	823.14	62.76	124.82	2.131
18	841.16	62.30	129.32	2.133
19	1087.50	63.62	160.00	2.137
20	1082.50	63.54	159.42	2.141
21	1049.51	63.56	154.42	2.141
22	741.92	62.36	113.24	2.144
23	1089.56	63.52	160.04	2.148
24	1961.30	84.12	164.24	2.148
25	837.89	62.90	125.40	2.149
26	1986.73	84.34	165.13	2.153
27	790.66	62.30	120.38	2.154
28	1986.77	84.00	166.00	2.159

Table 3.1 Dimensions and densities of rock salt prepared for uniaxial compression testing (cont.).

No.	Weight (g)	Diameter (mm)	Length (mm)	Density (g/cc)
29	766.46	62.40	116.04	2.159
30	811.21	62.56	122.16	2.159
31	2045.30	84.48	168.81	2.161
32	819.80	62.40	124.02	2.161
33	837.34	61.50	130.30	2.162
34	1764.72	83.76	147.50	2.170
35	1996.98	83.30	168.48	2.174
36	795.78	62.14	120.62	2.175
37	841.15	63.57	121.36	2.183
38	1951.12	83.45	163.19	2.185
39	1957.03	83.52	163.00	2.191
40	1906.12	81.10	168.19	2.193
41	1986.00	82.76	168.25	2.193
42	2060.77	83.62	170.20	2.204
43	1940.15	83.74	159.57	2.207
44	1693.37	84.30	137.30	2.209
45	1761.72	80.12	158.00	2.211
46	2029.02	81.78	174.62	2.211
47	2006.96	82.80	167.92	2.219
48	1955.93	82.40	164.63	2.227
49	2181.00	83.80	176.00	2.246
50	973.75	62.40	141.48	2.250
51	991.87	63.82	136.20	2.276

Twenty-two specimens are prepared for uniaxial creep test. Table 3.2 shows their dimensions and density.

Table 3.2 Dimension and density of rock salt prepared for uniaxial creep testing.

No.	Weight (g)	Diameter (mm)	Length (mm)	Density (g/cc)
1	735.61	61.90	118.10	2.069
2	802.95	62.20	126.28	2.092
3	740.43	62.86	113.64	2.099
4	877.39	63.24	132.80	2.103
5	738.68	62.80	113.10	2.108
6	771.61	62.75	117.29	2.127
7	780.84	62.40	119.84	2.130
8	807.72	62.42	123.40	2.138
9	859.38	62.60	129.70	2.152
10	2008.76	84.24	167.20	2.155
11	756.84	62.80	113.10	2.160
12	2057.49	84.11	171.35	2.160
13	1977.52	84.52	161.54	2.181
14	2047.98	83.80	169.26	2.193
15	2018.00	83.52	166.91	2.206
16	2085.49	83.94	170.67	2.207
17	915.94	63.10	132.30	2.213
18	873.35	62.30	129.40	2.213
19	2177.85	84.25	176.41	2.214
20	908.00	62.20	134.40	2.222
21	810.17	62.36	117.86	2.250
22	878.53	62.86	124.72	2.269

X-ray diffraction analysis is performed after the mechanical testing. The XRD analysis uses finely ground rock salt powder with particle sizes less than 0.25 mm (Figure 3.3). The X-ray diffraction (Bruker, D2 Phaser) is used.

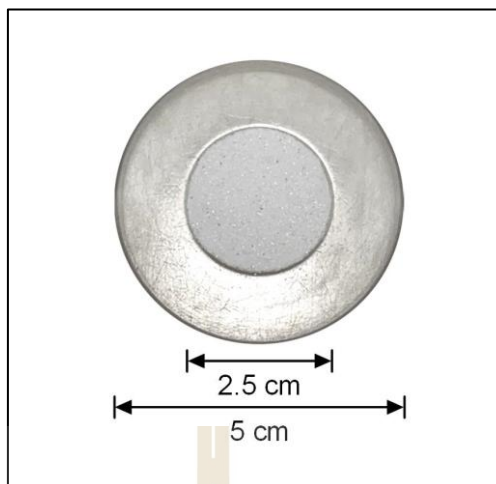
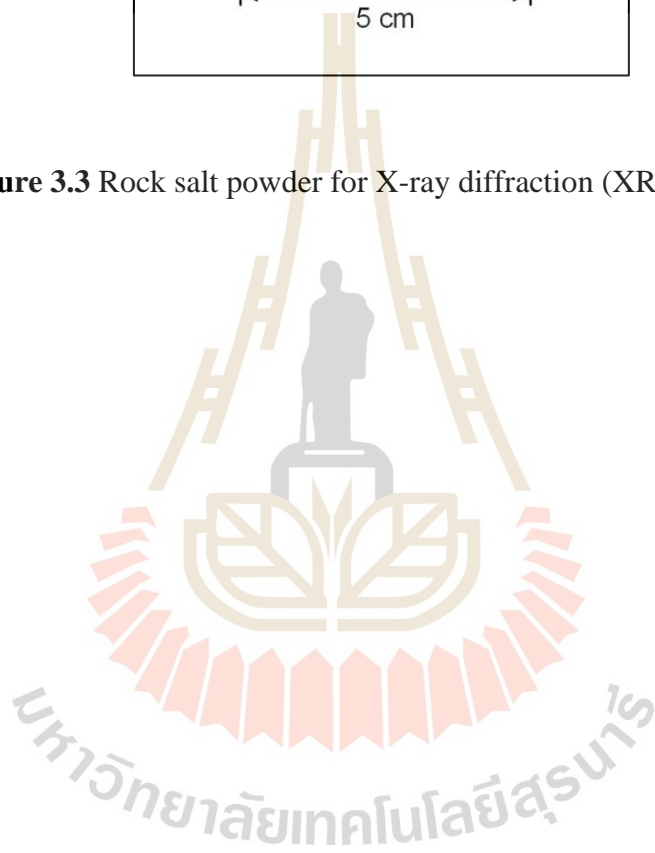


Figure 3.3 Rock salt powder for X-ray diffraction (XRD) analysis.



CHAPTER IV

LABORATORY TESTS METHOD AND RESULTS

4.1 Introduction

The laboratory tests performed in this study can be divided into three types: physical tests (density and wave velocity), mechanical tests (uniaxial compression and creep) and X-ray diffraction analysis (carnallite and anhydrite contents). All tests are conducted under the scope and limitations of the study proposed in the first chapter and sample preparation in the third chapter. This chapter describes the test methods and results.

4.2 Specimen

4.2.1 Density Measurements

The purpose of this test is to determine the density of each specimen. The rock salt specimens have been prepared according to the ASTM standard practice. Density is determined from the weight and volume of specimen; thus, general relationship is:

$$\rho = m/V \quad (4.1)$$

where ρ is density (g/cm^3 , g/cc)

m is weight (g)

V is volume (cm^3)

4.2.2 Density Results

The specimen volume (V) is calculated from an average of several caliper readings for four mutually perpendicular directions. Each caliper reading is to the nearest to 0.02 mm. The density (ρ) of rock salt ranges from 2.069 to 2.276 g/cc the average and standard deviation (SD) is 2.161 ± 0.046 g/cc. The density is an important factor controlling velocity of wave moving through the specimen. The density measurement results are shown in Table 4.1.

4.3 Ultrasonic Pulse Velocity (UPV)

4.3.1 Ultrasonic Pulse Velocity (UPV) Measurement Method

The purpose of this test is to obtain the wave velocities (P- and S-waves) moving through the specimens with different densities. OYO Sonic viewer 170 (Model 5338) is used. The application is carried out in accordance with ASTM D2845-08

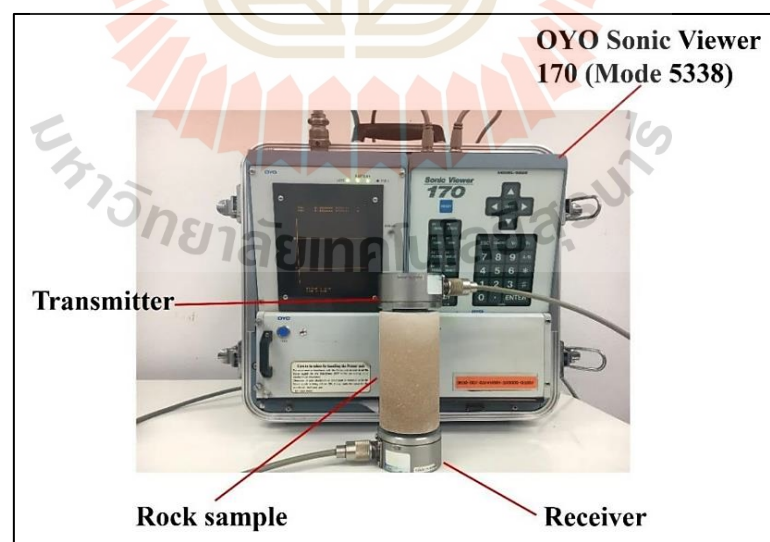


Figure 4.1 Direct method of ultrasonic pulse velocity measurements using by OYO Sonic viewer 170 Model 5338.

standard practice. Direct method was used in this study (Figure 4.1). The end surfaces of specimens are smooth cut to provide a good coupling between the transducer face and the specimens surface to maximize accuracy of the transit time measurements. Vaseline gel is applied as a coupling agent. The specimen lengths are approximately the same in order to minimize the time differences. Transmitter and receiver are held tightly at the end surfaces and then pulse transmitting time was measured. The dynamic young's modulus and Poisson's ratio are calculated using the following equations.

$$E_d = [\rho V_s^2(3V_p^2 - 4V_s^2)] / (V_p^2 - V_s^2) \quad (4.2)$$

$$v_d = (V_p^2 - 2V_s^2) / [2(V_p^2 - V_s^2)] \quad (4.3)$$

where E_d is dynamic Young's modulus (GPa)

v_d is dynamic Poisson's ratio

ρ is density (g/cm^3 , g/cc)

V_p is P-wave velocity (km/s)

V_s is S-wave velocity (km/s)

4.3.2 Ultrasonic Pulse Velocity (UPV) Results

The differences of the measured wave velocity are due to the difference of the density with in the specimens. Wave velocity through the specimen was calculated from one end to another. The P-wave velocity (V_p) of rock salt ranges from 4.45 to 5.71 km/s. The average and standard deviation (SD) are 5.16 ± 0.33 km/s. S-wave velocity (V_s) ranges from 2.04 to 3.17 km/s. The average and standard deviation (SD) are 2.67 ± 0.29 km/s. Dynamic elastic modulus (E_d) ranges from 23.58 to 58.16 GPa the average and standard deviation (SD) is 41.11 ± 8.80 GPa and dynamic

Poisson's ratio (ν_d) ranges from 0.26 to 0.37 the average and standard deviation (SD) is 0.32 ± 0.03 . The ultrasonic pulse velocity (V_p and V_s) measurement results are shown in Table 4.1.

Table 4.1 Ultrasonic pulse velocities and dynamic parameter of salt specimens.

No.	Density, ρ (g/cc)	V_p (km/sec)	V_s (km/sec)	E_d (GPa)	ν_d
1	2.088	4.48	2.06	24.28	0.37
2	2.096	4.58	2.16	26.63	0.36
3	2.100	4.70	2.27	29.12	0.35
4	2.100	4.45	2.37	31.79	0.34
5	2.107	4.95	2.38	32.24	0.35
6	2.114	4.94	2.56	33.81	0.34
7	2.115	5.30	2.65	39.56	0.33
8	2.118	5.36	2.84	44.65	0.30
9	2.121	5.13	2.53	36.48	0.34
10	2.123	5.34	2.79	43.46	0.31
11	2.123	5.15	2.45	34.37	0.35
12	2.123	5.02	2.53	36.22	0.33
13	2.126	5.16	2.59	38.07	0.33
14	2.127	4.84	2.42	33.28	0.33
15	2.130	5.20	2.49	35.74	0.35
16	2.130	5.19	2.54	36.99	0.34
17	2.131	5.33	2.60	38.74	0.34
18	2.133	5.48	2.81	44.55	0.32
19	2.137	4.55	2.29	29.60	0.33
20	2.141	4.57	2.28	29.77	0.33
21	2.141	4.68	2.30	30.48	0.34
22	2.144	4.72	2.48	34.60	0.31
23	2.148	4.85	2.35	32.02	0.35
24	2.148	4.98	2.42	33.73	0.35
25	2.149	5.23	2.73	41.95	0.31
26	2.153	5.00	2.58	37.80	0.32

Table 4.1 Ultrasonic pulse velocities and dynamic parameter of salt specimens (cont.).

No.	Density, ρ (g/cc)	V_p (km/sec)	V_s (km/sec)	E_d (GPa)	ν_d
27	2.154	5.02	2.56	37.40	0.32
28	2.159	5.19	2.59	38.73	0.33
29	2.159	4.76	2.52	35.84	0.30
30	2.159	5.55	2.71	42.74	0.34
31	2.161	5.45	2.77	43.88	0.33
32	2.161	5.00	2.65	39.59	0.30
33	2.162	5.25	2.83	44.94	0.30
34	2.170	4.92	2.63	39.11	0.30
35	2.174	5.27	2.72	42.33	0.32
36	2.175	5.48	2.81	45.27	0.32
37	2.183	5.52	2.89	47.79	0.31
38	2.185	5.26	2.81	44.98	0.30
39	2.191	5.09	2.67	40.99	0.31
40	2.193	5.26	2.80	44.85	0.30
41	2.193	5.26	2.85	46.08	0.29
42	2.204	5.32	2.84	46.15	0.30
43	2.207	5.54	3.01	51.63	0.29
44	2.209	5.49	2.98	50.79	0.29
45	2.211	5.27	2.98	49.68	0.26
46	2.211	5.46	3.06	52.71	0.27
47	2.219	5.60	3.05	53.29	0.29
48	2.227	5.68	3.12	55.60	0.28
49	2.246	5.71	3.10	55.71	0.29
50	2.250	5.66	3.12	56.03	0.28
51	2.276	5.68	3.17	58.16	0.27
52	2.069	4.54	2.04	23.58	0.37
53	2.092	4.86	2.30	29.91	0.36
54	2.099	4.94	2.37	31.78	0.35
55	2.103	4.74	2.29	29.72	0.35
56	2.108	4.92	2.36	31.62	0.35
57	2.127	4.93	2.44	33.95	0.34
58	2.130	4.91	2.45	34.02	0.34

Table 4.1 Ultrasonic pulse velocities and dynamic parameter of salt specimens (cont.).

No.	Density, ρ (g/cc)	V_p (km/sec)	V_s (km/sec)	E_d (GPa)	ν_d
59	2.138	4.94	2.50	35.43	0.33
60	2.152	4.99	2.54	36.80	0.32
61	2.155	5.10	2.70	40.92	0.31
62	2.160	5.19	2.70	41.30	0.31
63	2.160	5.13	2.72	41.69	0.30
64	2.181	5.21	2.79	43.99	0.30
65	2.193	5.29	2.82	45.42	0.30
66	2.206	5.38	2.88	47.50	0.30
67	2.207	5.51	2.97	50.51	0.29
68	2.213	5.56	3.02	52.11	0.29
69	2.213	5.53	3.07	53.19	0.28
70	2.214	5.55	3.09	54.03	0.27
71	2.222	5.60	3.10	54.55	0.28
72	2.250	5.61	3.15	56.74	0.27
73	2.269	5.67	3.17	57.90	0.27

4.4 Mechanical Test

4.4.1 Uniaxial Compression Testing Method

The purpose of this test is to determine the mechanical properties of the tested rock salt. The uniaxial compression test is carried out to determine uniaxial compressive strength, static elastic modulus and static Poisson's ratio. The procedure follows the ASTM D7012-14 standard practice. The compression load frame is used (Figure 4.2). Each specimen is axially loaded with a loading rate of 0.1 MPa/sec until failure, then the compressive strength is calculated by dividing the maximum load by the original cross-sectional area following this equation:

$$\sigma_c = P/A \quad (4.4)$$

where σ_c is uniaxial compressive strength (MPa)

P is failure load (N/m²)

A is initial cross-sectional area (m²)

The static elastic modulus and Poisson's ratio are calculated by:

$$E = \sigma_1 / \epsilon_1 \quad (4.5)$$

$$\nu = \epsilon_3 / \epsilon_1 \quad (4.6)$$

where E is static elastic modulus (GPa)

ν is static Poisson's ratio

σ_1 is axial stress (MPa)

ϵ_1 is axial strain

ϵ_3 is lateral strain

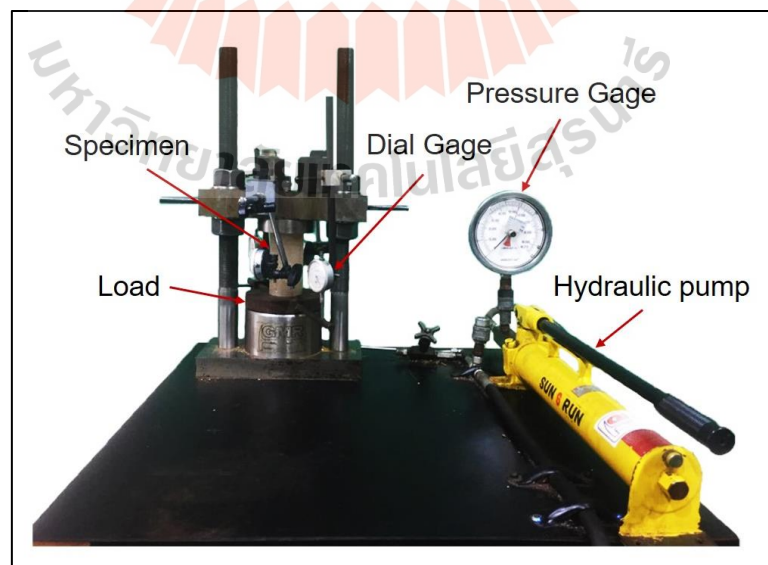


Figure 4.2 Uniaxial compression test device.

4.4.2 Uniaxial Compression Results

Fifty-one specimens have been tested. The elastic modulus and Poisson's ratio are calculated from the stress-strain curves at about 50% of the maximum stress level (Figures 4.3 to 4.6). The results from this test with standard deviations are shown in Table 4.2. The uniaxial compressive strength (σ_c) of rock salt ranges from 15.94 to 37.51 MPa with the average and standard deviation (SD) of 27.64 ± 4.70 MPa. The static elastic modulus (E) ranges from 1.15 to 2.20 GPa with the average and standard deviation (SD) of 1.57 ± 0.31 GPa. The static Poisson's ratio (ν) ranges from 0.23 to 0.38 with the average and standard deviation (SD) of 0.31 ± 0.04 .

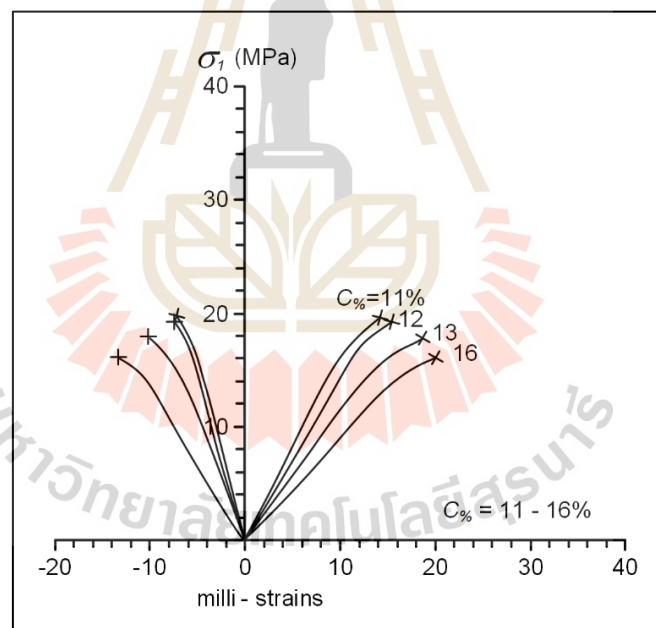


Figure 4.3 Stress-stain curves from uniaxial compression tests of salt specimens with

$C\% = 11-16\%$.

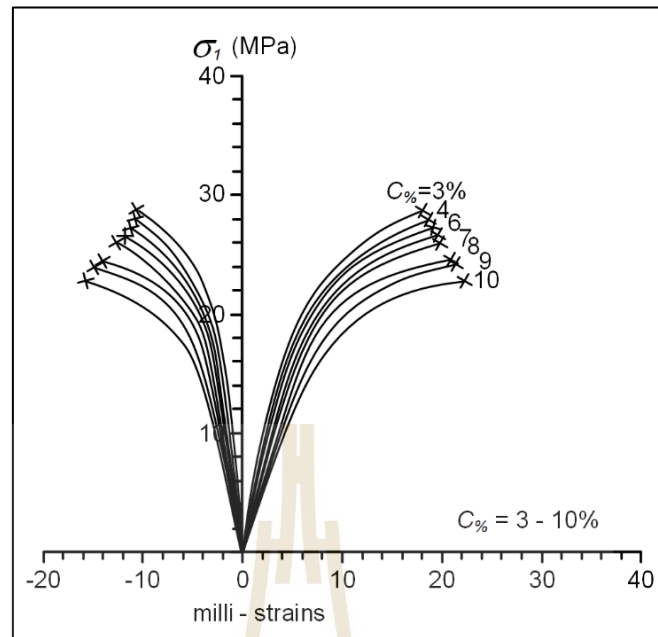


Figure 4.4 Stress-stain curves from uniaxial compression tests of salt specimens with $C\% = 3-10\%$.

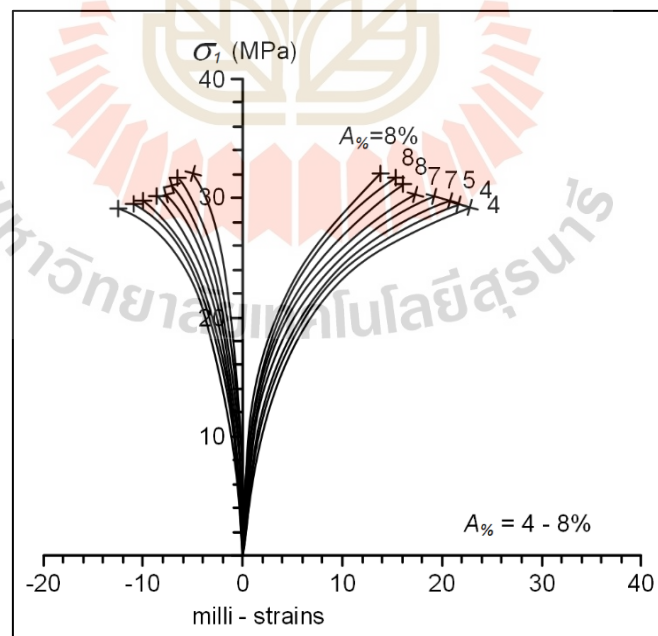


Figure 4.5 Stress-stain curves from uniaxial compression tests of salt specimens with $A\% = 4-8\%$.

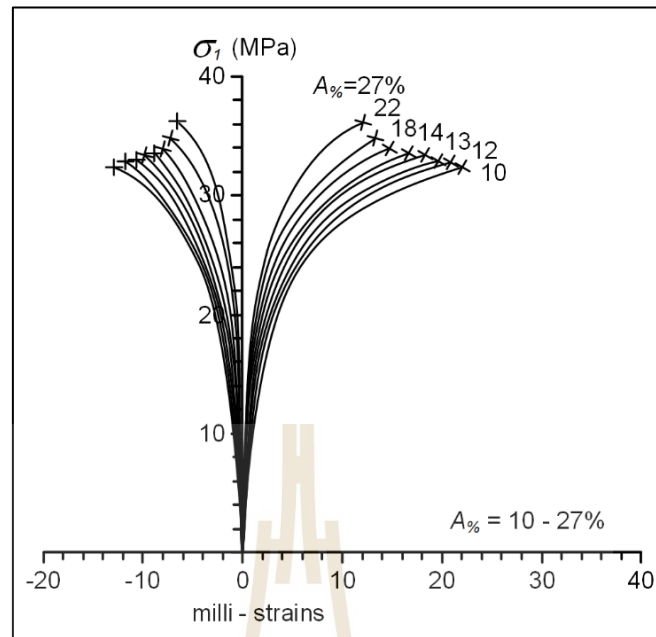


Figure 4.6 Stress-stain curves from uniaxial compression tests of salt specimens with $A_{\%} = 10-27\%$.

Table 4.2 Results from the uniaxial compression test.

No.	σ_c (MPa)	E (GPa)	ν	No.	σ_c (MPa)	E (GPa)	ν
1	15.94	1.02	0.38	27	27.88	5.45	0.31
2	17.70	1.60	0.37	28	27.97	5.78	0.32
3	19.07	1.83	0.36	29	28.61	6.51	0.31
4	19.15	1.93	0.34	30	27.65	5.24	0.33
5	19.46	2.10	0.35	31	28.54	6.37	0.31
6	22.74	2.35	0.32	32	29.43	7.57	0.33
7	24.06	2.68	0.33	33	28.61	6.67	0.32
8	24.31	2.82	0.31	34	29.04	7.08	0.30
9	23.79	2.24	0.32	35	29.36	7.37	0.29
10	23.91	2.51	0.32	36	29.68	7.60	0.29
11	24.21	2.75	0.34	37	29.93	7.91	0.28
12	25.28	3.02	0.33	38	30.17	8.31	0.29
13	25.51	3.21	0.31	39	31.03	9.28	0.30

Table 4.2 Results from the uniaxial compression test (cont.).

No.	σ_c (MPa)	E (GPa)	ν	No.	σ_c (MPa)	E (GPa)	ν
14	24.09	2.70	0.34	40	31.94	11.01	0.29
15	25.93	3.66	0.35	41	31.60	10.76	0.28
16	26.10	4.32	0.32	42	32.78	12.76	0.27
17	25.86	3.36	0.34	43	32.68	12.37	0.26
18	26.24	4.81	0.31	44	32.25	12.72	0.26
19	25.36	3.80	0.32	45	33.72	13.90	0.25
20	26.05	4.42	0.31	46	33.32	13.44	0.24
21	27.38	5.45	0.33	47	33.43	13.52	0.27
22	26.19	4.37	0.33	48	34.69	14.21	0.23
23	27.25	5.57	0.34	49	35.30	15.35	0.23
24	26.09	4.43	0.33	50	35.97	15.93	0.25
25	27.35	5.09	0.33	51	37.51	19.18	0.23
26	27.74	5.28	0.33				

4.5 Creep Test

4.5.1 Uniaxial Creep Test Method

The uniaxial creep test is carried out on twenty-two salt specimens to determine time-dependent behavior of specimens. The tested specimens had been measured for their sizes, density and ultrasonic pulse velocity. The procedure follows the ASTM D7070-08 standard practice. The specimens are tested under constant axial stress of 10 MPa for up to 10 days. The dial gages are installed to measure the axial and lateral deformations (Figure 4.7). The time-related displacements are recorded.

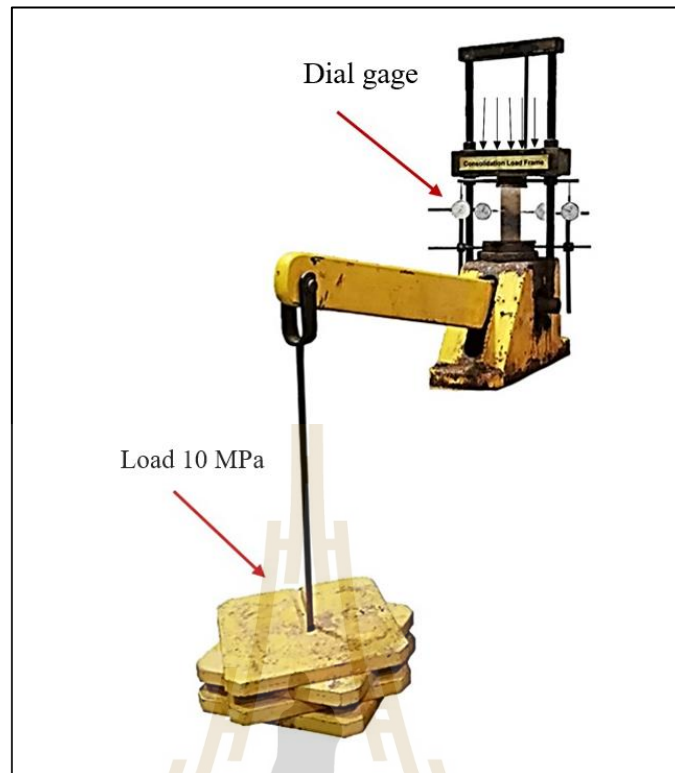


Figure 4.7 Uniaxial creep test device.

4.5.2 Creep Property Results

Twenty-two specimens have been tested. The results from uniaxial creep tests are shown in Figures 4.8 and 4.9. They present the time-dependent deformation in the form of octahedral shear strains as a function of time (t) (Jaeger et al., 2007):

$$\gamma_{\text{oct}} = 1/3[(\epsilon_1 - \epsilon_2)^2 + (\epsilon_2 - \epsilon_3)^2 + (\epsilon_3 - \epsilon_1)^2]^{1/2} \quad (4.7)$$

where γ_{oct} is octahedral shear strains

ϵ_1 is axial strain

$\epsilon_2 = \epsilon_3$ are lateral strain

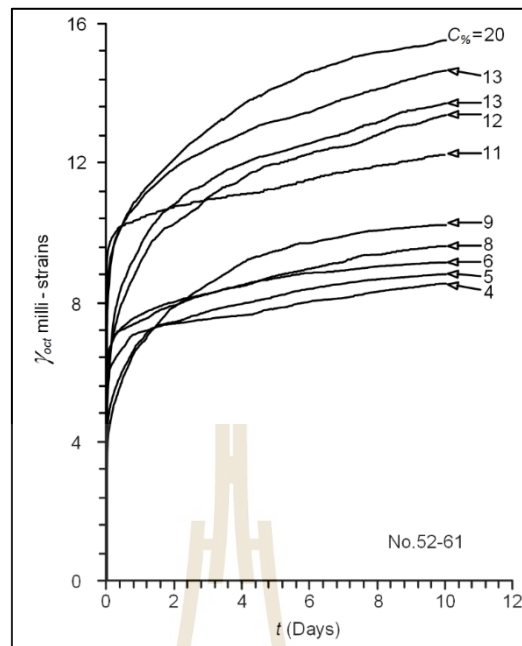


Figure 4.8 Octahedral shear strain as a function of $C\%$. Solid lines are test results. Dash lines are curve fits with Burgers model.

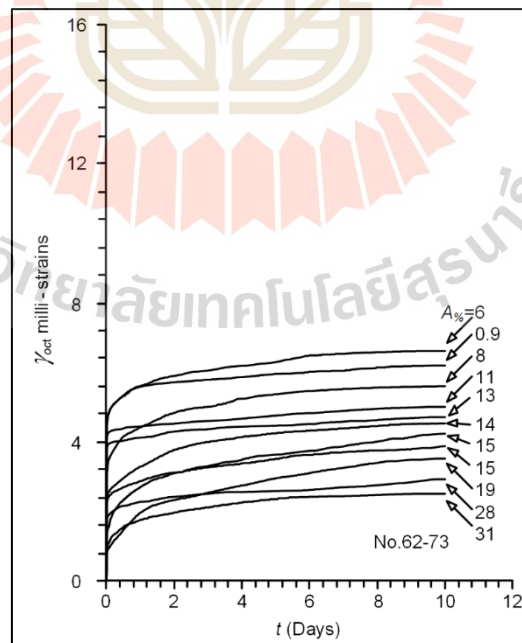


Figure 4.9 Octahedral shear strain as a function of $A\%$. Solid lines are test results. Dash lines are curve fits with Burgers model.

The strain results show the instantaneous, transient and steady-state creep behavior. Higher $C\%$ specimens show higher strains while higher $A\%$ specimens exhibit lower strains.

4.6 Mineral Compositions

4.6.1 X-ray Diffraction (XRD) Analysis

The mineral compositions of all salt specimens are determined after uniaxial compression test and uniaxial creep test. The X-ray diffraction (Bruker, D2 Phaser) is used (Figure 4.10).

4.6.2 X-ray Diffraction (XRD) Results

The results can be used to identify the effect of inclusions (impure rock salt) among the salt specimens. The results indicate that halite content ($H\%$) of rock salt range from 66.00 to 98.90% with the average and standard deviation (SD) of $88.30 \pm 6.96\%$. The anhydrite content ($A\%$) range from 0.00 to 32.19% with the average



Figure 4.10 X-ray diffraction Bruker, D2 Phaser (The Center for Scientific and Technology Equipment, Suranaree University of Technology).

and standard deviation (SD) of $5.57 \pm 8.46\%$. The carnallite content $C\%$ ranges from 0.00 to 20.28% with the average and standard deviation (SD) of $4.66 \pm 4.96\%$. The trace minerals (sylvite, gypsum, tachyhydrite, montmorillonite, illite and kaolinite) range from 0.49 to 1.98% with the average and standard deviation (SD) of $1.47 \pm 0.43\%$. The results from X-ray diffraction analysis are shown in Table 4.3 and Table 4.4.

Table 4.3 Result of X-ray diffraction analyses of uniaxial compression test.

No.	H% (%)	A% (%)	C% (%)	Trace minerals (%)
1	82.30	0.16	16.08	1.46
2	85.75	0.00	13.10	1.15
3	86.33	0.00	12.40	1.27
4	86.83	0.00	12.24	0.93
5	86.46	0.27	11.30	1.97
6	88.66	0.17	10.16	1.01
7	89.29	0.06	9.61	1.04
8	89.89	0.15	9.07	0.89
9	88.96	0.20	8.90	1.94
10	89.81	0.05	8.85	1.29
11	89.66	0.01	8.81	1.52
12	89.21	0.19	8.76	1.84
13	89.23	0.25	8.67	1.85
14	89.69	0.29	8.24	1.78
15	89.84	0.45	7.81	1.90
16	90.43	0.14	7.52	1.91
17	91.45	0.01	7.43	1.11
18	91.07	0.03	7.21	1.69
19	92.46	0.01	6.65	0.88
20	92.99	0.01	6.18	0.82
21	92.87	0.24	6.04	0.85
22	92.36	0.13	5.58	1.93
23	92.66	0.09	5.36	1.89
24	92.80	0.27	5.29	1.64

Table 4.3 Result of X-ray diffraction analyses of uniaxial compression test (cont.).

No.	H% (%)	A% (%)	C% (%)	Trace minerals (%)
25	92.65	0.24	5.15	1.96
26	93.51	0.55	4.63	1.31
27	94.08	0.36	4.24	1.32
28	94.09	0.48	3.61	1.82
29	95.86	0.00	3.43	0.71
30	94.94	0.00	3.27	1.79
31	96.94	1.24	0.00	1.82
32	97.39	1.54	0.18	0.89
33	96.49	1.71	0.00	1.80
34	94.42	3.66	0.00	1.92
35	93.83	4.38	0.00	1.79
36	93.31	4.87	0.02	1.80
37	92.06	6.50	0.02	1.42
38	92.30	6.71	0.13	0.86
39	90.97	7.55	0.00	1.48
40	90.97	8.14	0.00	0.89
41	89.70	8.39	0.00	1.91
42	88.37	10.00	0.00	1.63
43	86.33	11.96	0.02	1.69
44	85.22	13.24	0.11	1.43
45	85.05	13.74	0.01	1.20
46	84.07	13.95	0.00	1.98
47	81.12	17.81	0.03	1.04
48	77.30	21.61	0.06	1.03
49	73.94	24.07	0.02	1.97
50	71.32	26.74	0.05	1.89
51	66.00	32.19	0.08	1.73

Table 4.4 Result of X-ray diffraction analyses of uniaxial creep test.

No.	H% (%)	A% (%)	C% (%)	Trace minerals (%)
52	78.06	0.02	20.28	1.64
53	84.85	0.03	13.14	1.98
54	85.92	0.04	12.67	1.37
55	86.78	0.03	11.83	1.36
56	87.88	0.02	11.22	0.88
57	90.34	0.00	8.55	1.11
58	91.44	0.02	7.66	0.88
59	91.98	0.00	6.48	1.54
60	93.99	0.00	4.82	1.19
61	95.01	0.07	4.15	0.77
62	98.90	0.52	0.05	0.53
63	98.58	0.85	0.08	0.49
64	91.74	6.35	0.05	1.86
65	89.94	7.91	0.20	1.95
66	87.88	10.72	0.09	1.31
67	85.47	12.61	0.07	1.85
68	83.75	14.43	0.03	1.79
69	83.31	14.86	0.08	1.75
70	82.80	15.34	0.06	1.80
71	78.66	19.49	0.14	1.71
72	67.40	28.24	2.45	1.91
73	67.68	30.57	0.07	1.68

CHAPTER V

DEVELOPMENT OF MATHEMATICAL RELATIONSHIPS

5.1 Introduction

The purpose of this chapter is to determine the relationships between wave velocities (P- and S-waves), mechanical properties and mineral compositions of the studied rock salt specimens under different amount of carnallite and anhydrite contents. Mechanical properties include uniaxial compressive strength, elastic modulus, Poisson's ratio, spring constant in visco-elastic phase, visco-plastic viscosity and visco-elastic viscosity.

5.2 Relationship between Pulse Velocity and Density

The linear relationships are proposed to correlate the P- and S-wave velocities with the specimen density. The results indicate that increasing of density will increase P- and S-wave velocities. Good correlations are obtained from both wave velocities ($R^2 = 0.606$ and $R^2 = 0.804$), as shown in Figure 5.1. The increase of the wave velocities and density is may be due to the inclusion of anhydrite. The following equations define this relationship:

$$V_p = 5.574 \cdot \rho - 6.882 \quad \text{km/s} \quad (5.1)$$

$$V_s = 5.523 \cdot \rho - 9.261 \quad \text{km/s} \quad (5.2)$$

where ρ is density (g/cm^3 , g/cc)

V_p is P-wave velocity (km/s)

V_s is S-wave velocity (km/s)

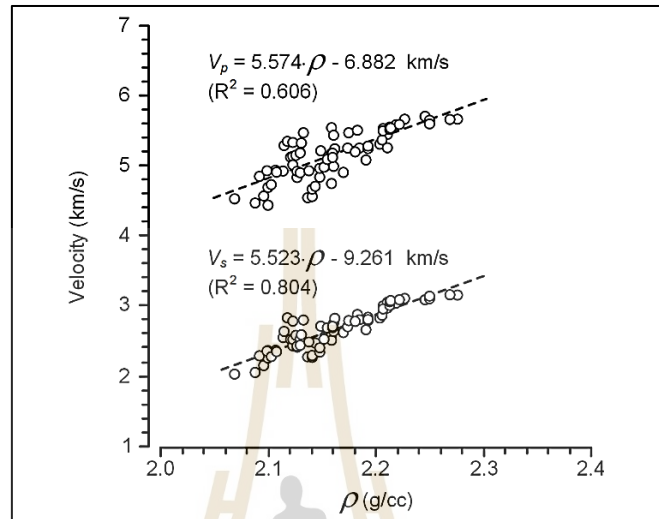


Figure 5.1 Relationship between P- and S-wave velocities and density.

The P-wave velocities can be correlated with the S-wave velocities using a linear equation. The results indicate that P-wave velocities increases with increasing S-wave velocities, as shown in Figure 5.2.

$$V_p = 1.078 \cdot V_s - 2.281 \quad \text{km} \quad (5.3)$$

The relation between the two wave types suggests that the UPV measurements are reliable.

5.3 Relationship between Dynamic Properties and Density

The dynamic young's modulus can be well correlated with the density using a linear equation. The dynamic elastic modulus increases with increasing density. The relationship are shown in Figure 5.3, with their mathematic relation showing below:

$$E_d = 176.06 \cdot \rho - 335.07 \quad \text{GPa} \quad (5.4)$$

where E_d is dynamic young's modulus (GPa). The coefficient of correlation (R^2) is 0.844.

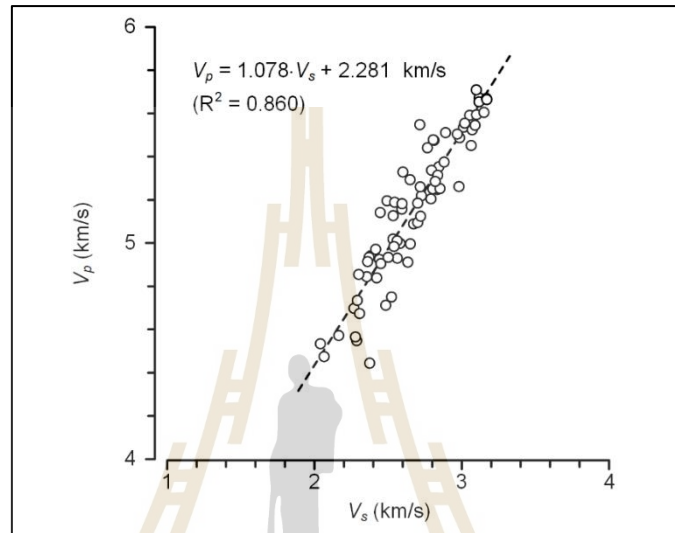


Figure 5.2 Relationship between P-wave and S-wave velocities.

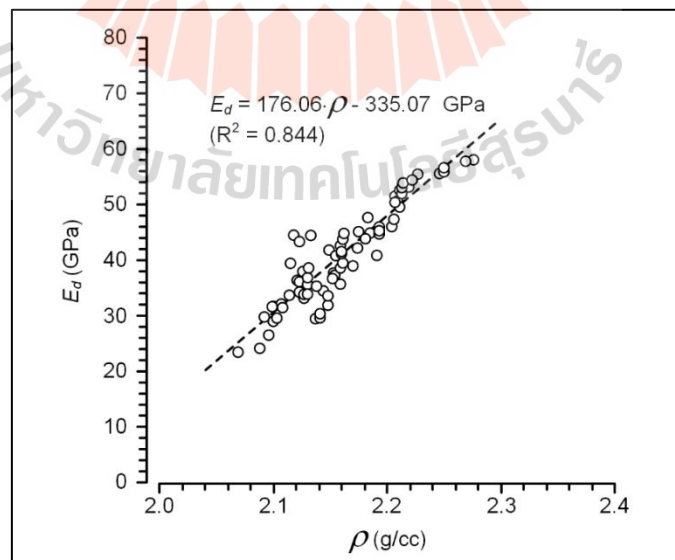


Figure 5.3 Relationship between dynamic elastic modulus and density.

The dynamic Poisson's ratio can also be correlated with the density using a linear equation. The dynamic Poisson's ratio decreases with increasing density, suggesting that as the salt specimens become denser, they exhibit lower dilation behavior (Poisson's ratio decreases). The linear relationship are shown in Figure 5.4. The relationship can be represented by:

$$v_d = -0.526 \cdot \rho + 1.453 \quad (5.5)$$

where v_d is dynamic Poisson's ratio. The coefficient of correlation (R^2) is 0.794.

The dynamic elastic modulus can be correlated with the P- and S-wave velocities using linear equations. Increasing of P- and S-wave velocities will increase dynamic elastic modulus. The following equations represented their relationships.

$$E_d = 24.613 \cdot V_p - 85.986 \quad \text{GPa} \quad (5.6)$$

$$E_d = 30.613 \cdot V_s - 40.763 \quad \text{GPa} \quad (5.7)$$

Good correlation is obtained from both wave velocities, as shown in Figure 5.5. The increase of the wave velocities and dynamic elastic modulus is probably due to the inclusion of anhydrite.

The dynamic Poisson's ratio can also be correlated with the P- and S-wave velocities. The dynamic Poisson's ratio decreases linearly with increasing P- and S-wave velocities.

$$v_d = -0.059 \cdot V_p - 0.621 \quad (5.8)$$

$$v_d = -0.088 \cdot V_s + 40.763 \quad (5.9)$$

Good correlation is obtained from both P- and S-wave velocities ($R^2 = 0.512$ and $= 0.834$), as shown in Figure 5.6.

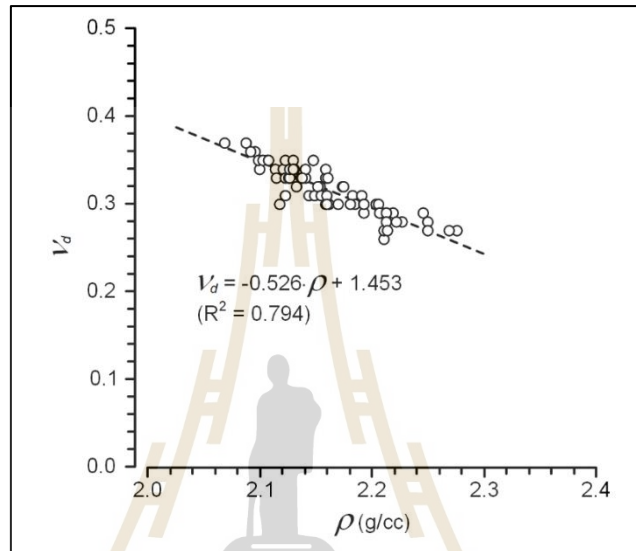


Figure 5.4 Relationship between dynamic Poisson's ratio and density.

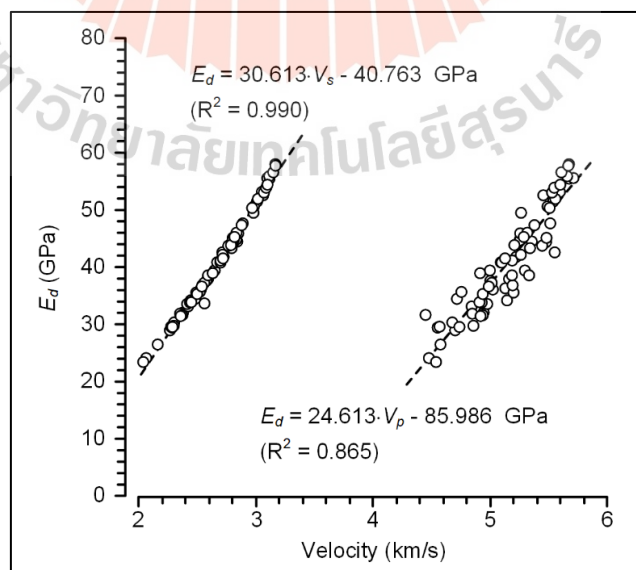


Figure 5.5 Relationship between dynamic young's modulus and P- and S-wave velocities.

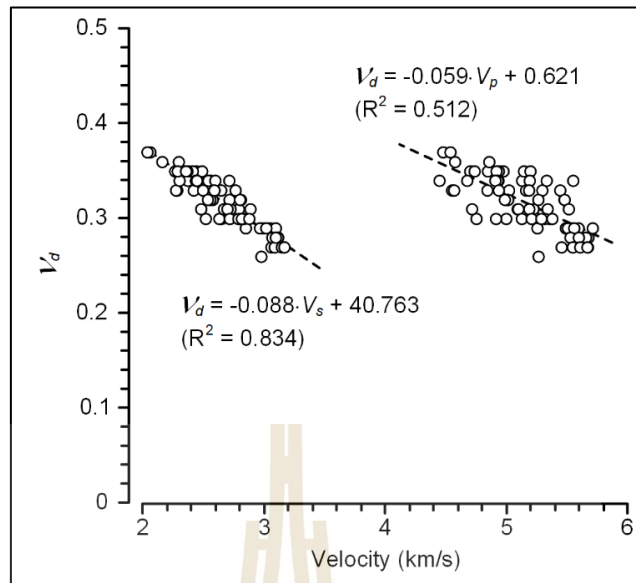


Figure 5.6 Relationship between dynamic Poisson's ratio and P- and S-wave velocities.

5.4 Relationship between Mechanical Properties and Densities

The linear relationship can represent the uniaxial compressive strength as a function of specimen density. The results indicate that salt density increases with the salt strength. The relationship are shown in Figure 5.7:

$$\sigma_c = 105.66 \cdot \rho - 200.45 \quad \text{MPa} \quad (5.11)$$

where σ_c is uniaxial compressive strength (MPa). Very good correlation is obtained ($R^2 = 0.926$).

The static elastic modulus can also be described by the specimen density using a linear equation. The increasing of density will increase the specimen stiffness, as shown in Figure 5.8. The E- ρ relation is given below:

$$E = 102.85 \cdot \rho - 215.31 \quad \text{GPa} \quad (5.12)$$

where E is static elastic modulus (GPa). Again, very good correlation is obtained ($R^2 = 0.965$).

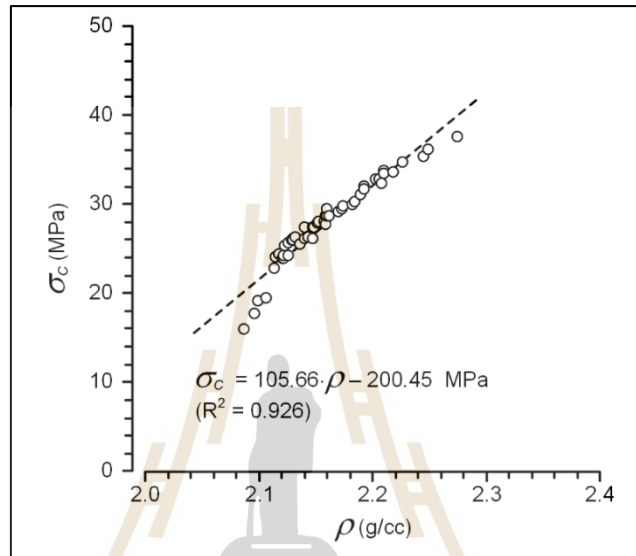


Figure 5.7 Relationship between uniaxial compressive strength and density.

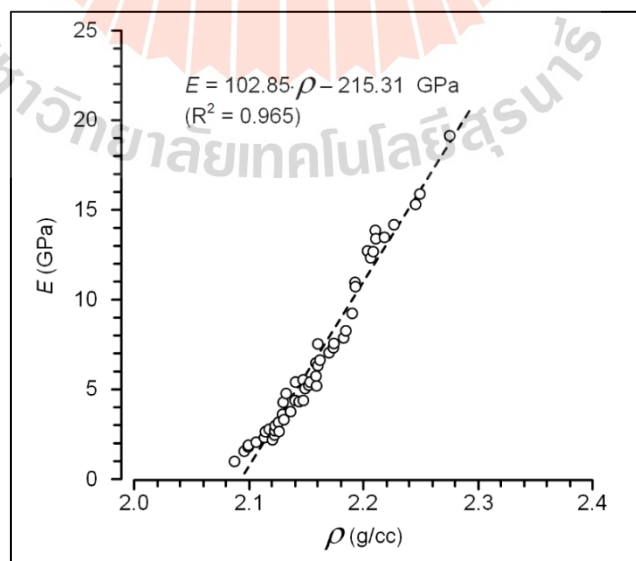


Figure 5.8 Relationship between static elastic modulus and density.

The static Poisson's ratio decreases with increasing density which can be described by a linear equation. This is probably due to the fact that the anhydrite inclusions make the specimen denser and lead to lower dilation behavior. The relationship are shown in Figure 5.9:

$$\nu = -0.776 \cdot \rho + 1.982 \quad (5.13)$$

where ν is static Poisson's ratio.

5.5 Relationship between Mechanical and Dynamic Properties

An attempt is made have to correlate the mechanical properties of salt specimens with the dynamic properties under different inclusion contents. The linear relationships are used to define the uniaxial compressive strength as a function of the P- and S-wave velocities. The results indicate P- and S-wave velocities increase with the uniaxial compressive strength. The following equations define their relations:

$$\sigma_c = 9.984 \cdot V_p - 23.814 \quad \text{MPa} \quad (5.14)$$

$$\sigma_c = 14.930 \cdot V_s - 12.098 \quad \text{MPa} \quad (5.15)$$

Good correlations ($R^2 = 0.514$ and $R^2 = 0.721$) are obtained from both wave velocities, as shown in Figure 5.10.

The static elastic modulus can also define as a function of be the dynamic young's modulus using a linear equation. A positive correlation is obtained as shown in

Figure 5.11. Note that the dynamic Young's modulus is about 10 to 20 times of the static elastic modulus.

$$E = 0.473 \cdot E_d + 12.492 \quad \text{GPa} \quad (5.16)$$

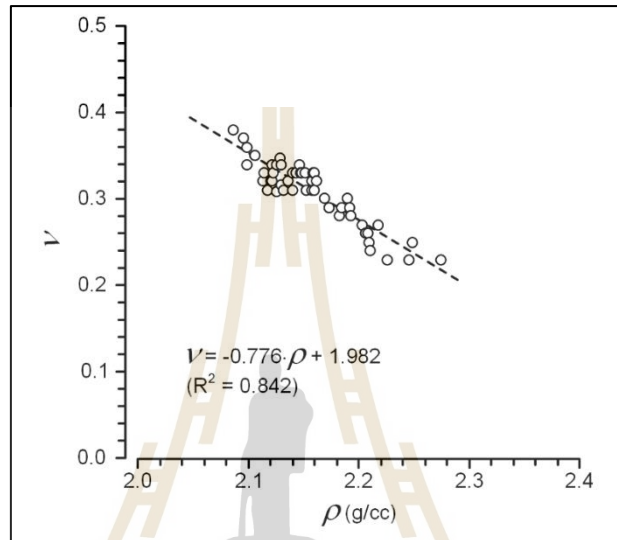


Figure 5.9 Relationship between static Poisson's ratio and density.

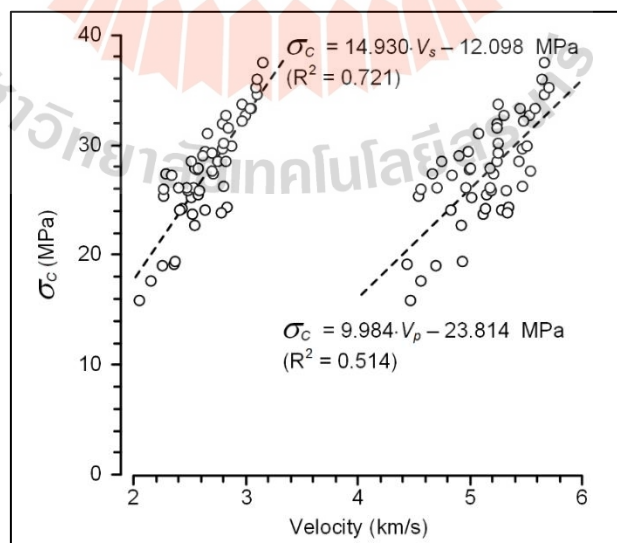


Figure 5.10 Relationship between uniaxial compressive strength and P- and S-wave velocities.

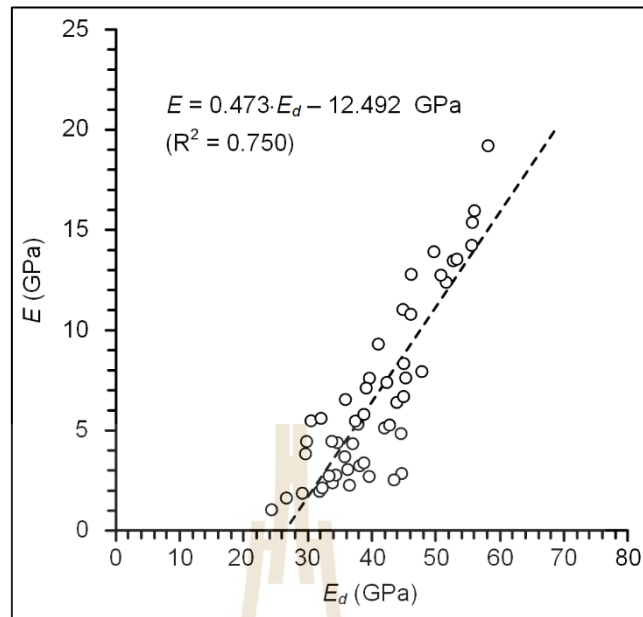


Figure 5.11 Relationship between static elastic modulus and dynamic elastic modulus.

Similarly, the static Poisson's ratio can be defined as a function of the dynamic Poisson's ratio using a linear equation. The relationship is shown in Figure 5.12, with a good correlation. The Poisson's ratios obtained from both methods tend to be comparable.

$$\nu = 1.265 \cdot \nu_d - 1.982 \quad (5.17)$$

5.6 Calibration of Creep Parameters

The Burgers model (Skrzypek and Hetnarski, 1993) is used to describe the time-dependent deformation of the creep test specimens. It is used because it is simple and capable of describing the elastic, visco-elastic, and visco-plastic phases of deformation.

The governing equation for uniaxial creep test under constant deviatoric stresses and confining pressure can be developed, representing the time-dependent strains as a function of time as follows (Skrzypek and Hetnarski, 1993):

$$\gamma_{\text{oct}}(t) = \tau_{\text{oct}}[(t/\eta_1) + (1/E_1) + (1/E_2) \cdot (1 - \exp(E_2 \cdot t/\eta_2))] \quad (5.18)$$

where t is the testing time

E_1 is the elastic modulus

E_2 is the spring constant in visco-elastic phase

η_1 is the viscosity coefficient in steady-state phase

η_2 is the viscosity coefficient in transient phase

Regression analyses on the strain-time curves based on Equation (5.18) using the SPSS statistical software (Wendai 2000) can determine the Burgers parameters for each specimen.

The spring constant (E_1) of rock salt ranges from 0.55 to 4.36 GPa. The spring constant in visco-elastic phase (E_2) ranges from 1.14 to 3.63 GPa. The visco-plastic viscosity (η_1) ranges from 16.01 to 500.15 GPa·day. The visco-elastic (η_2) ranges from 1.74 to 6.66 GPa·day. The results from calibration of uniaxial creep test data are shown in Table 5.1.

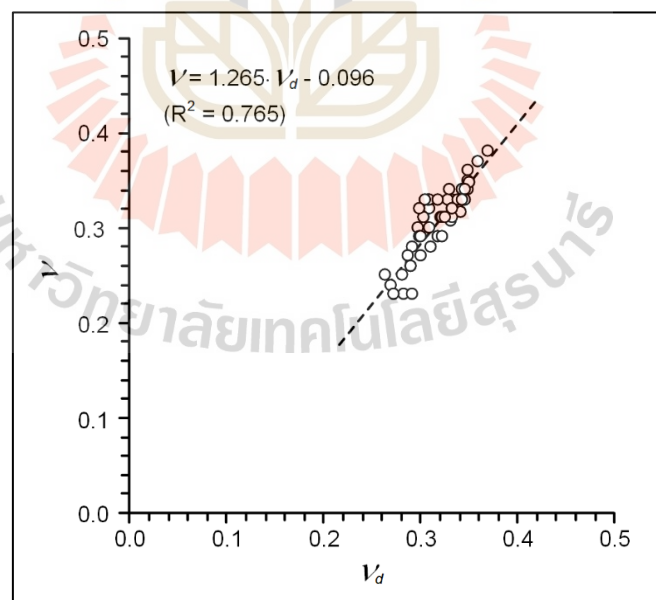
Table 5.1 Results from calibration of uniaxial creep test data against Burgers model.

No.	E_1 (GPa)	E_2 (GPa)	η_1 (GPa·day)	η_2 (GPa·day)
52	0.55	1.14	16.01	1.74
53	0.57	1.15	24.02	1.51
54	0.66	0.98	29.06	1.59
55	0.65	1.04	31.99	2.33
56	0.49	4.20	35.04	7.25
57	1.16	0.92	44.83	1.47
58	0.72	2.22	48.51	5.54
59	0.73	2.66	53.26	3.46
60	1.06	1.37	57.24	1.30

Table 5.1 Results from calibration of uniaxial creep test data against Burgers model.

(Cont.)

No.	E_1 (GPa)	E_2 (GPa)	η_1 (GPa·day)	η_2 (GPa·day)
61	0.84	2.51	60.05	2.05
62	1.70	1.00	64.99	3.49
63	0.81	3.57	85.50	2.11
64	1.01	3.38	79.84	3.85
65	1.40	2.60	100.73	3.44
66	1.11	11.58	130.20	39.27
67	1.21	9.00	166.47	18.76
68	1.93	2.61	184.57	4.55
69	2.75	2.21	190.54	4.90
70	1.83	4.61	200.57	13.92
71	3.77	2.20	251.20	7.41
72	2.42	6.37	398.33	13.76
73	4.36	3.63	500.15	6.66

**Figure 5.12** Static Poisson's ratio as a function of dynamic Poisson's ratio.

5.7 Correlations between Creep Parameters and Dynamic Properties

An exponential equation can be used to correlate the spring constant in instantaneous deformation mode with the P- and S-wave velocities. As the wave velocities increase, the spring constant will increase. The following equations define their relations:

$$E_I = 2 \times 10^{-4} \cdot \exp[1.691 \cdot V_p] \quad \text{GPa} \quad (5.19)$$

$$E_I = 0.013 \cdot \exp[1.665 \cdot V_s] \quad \text{GPa} \quad (5.20)$$

where E_I is the elastic modulus (GPa)

Good correlations are obtained from both wave velocities, as shown in Figure 5.13 ($R^2 = 0.772$ and $R^2 = 0.771$).

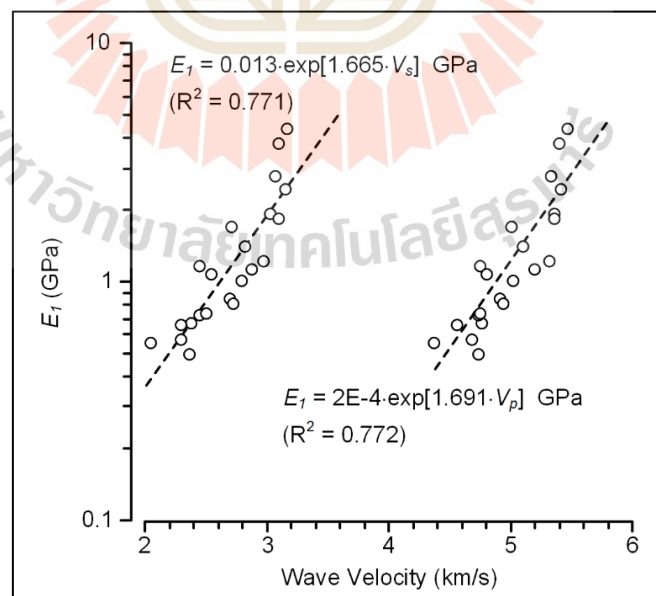


Figure 5.13 Relationship between the elastic modulus and P- and S-wave velocities.

The spring constant in visco-elastic phase also increases exponentially with the P- and S-wave velocities:

$$E_2 = 2.1 \times 10^{-3} \cdot \exp[1.366 \cdot V_p] \quad \text{GPa} \quad (5.21)$$

$$E_2 = 0.064 \cdot \exp[1.352 \cdot V_s] \quad \text{GPa} \quad (5.22)$$

where E_2 is the spring constant in visco-elastic phase (GPa). Poor correlations are however obtained from both wave velocities, as shown in Figure 5.14. Explanation will be given in the discussion section.

The visco-plastic coefficient (η_1) also increases with the P- and S-wave velocities. An exponential equation can define the relationship as:

$$\eta_1 = 6 \times 10^{-5} \cdot \exp[2.742 \cdot V_p] \quad \text{GPa-day} \quad (5.23)$$

$$\eta_1 = 0.053 \cdot \exp[2.725 \cdot V_s] \quad \text{GPa-day} \quad (5.24)$$

where η_1 is the visco-plastic coefficient (GPa-day). Very good correlation is obtained from both wave velocities, as shown in Figure 5.15. These equations will be very useful to assess the long-term deformation of the salt.

Poor correlations are obtained between η_2 and the wave velocities (Figure 5.16), where their relationships may be described by exponential equations:

$$\eta_2 = 2 \times 10^{-4} \cdot \exp[1.886 \cdot V_p] \quad \text{GPa-day} \quad (5.25)$$

$$\eta_2 = 0.035 \cdot \exp[1.781 \cdot V_s] \quad \text{GPa-day} \quad (5.26)$$

where η_2 is the visco-elastic viscosity (GPa·day)

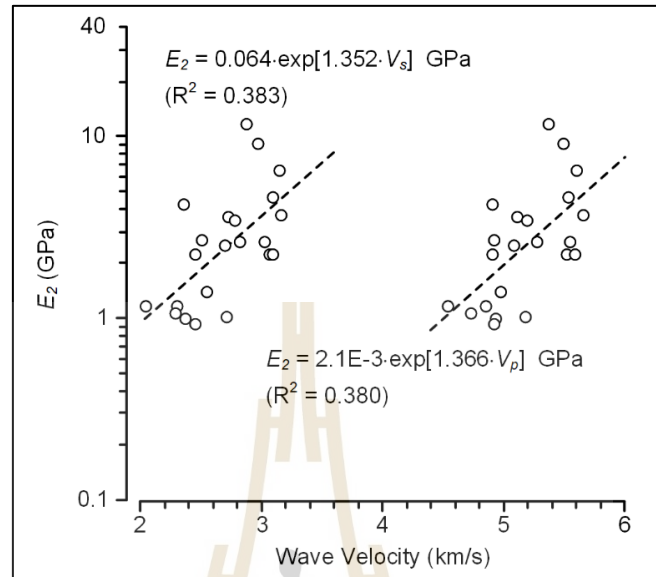


Figure 5.14 Spring constant in visco-elastic phase as a function of P- and S-wave velocities.

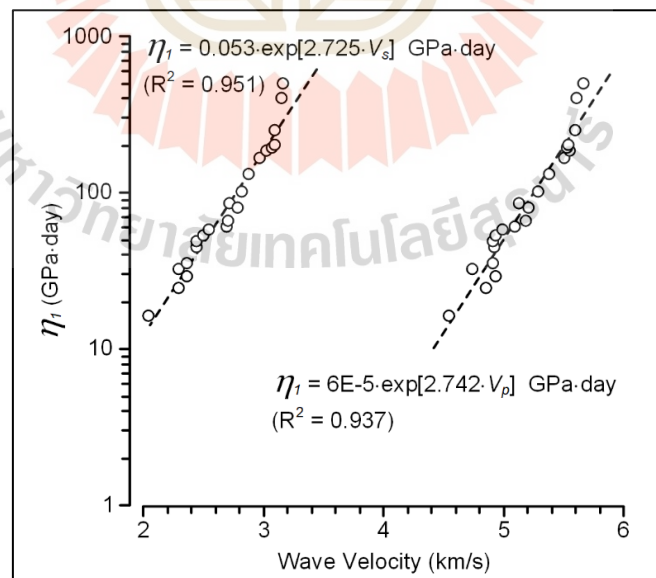


Figure 5.15 Relationship between the visco-plastic coefficient and P- and S-wave velocities.

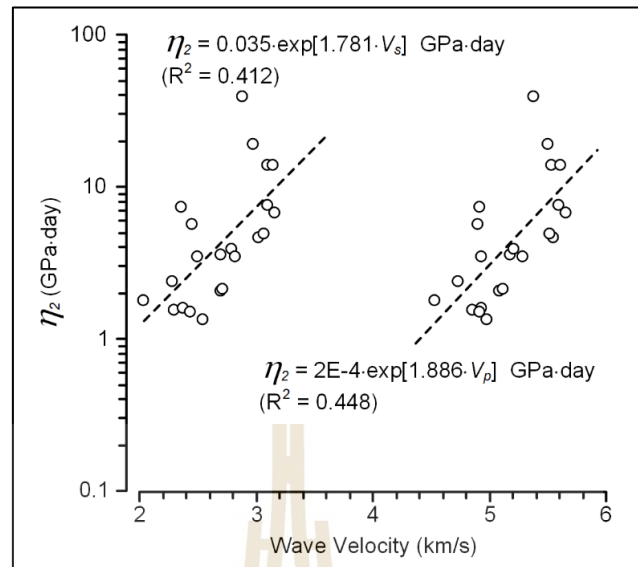


Figure 5.16 Relationship between the visco-elastic viscosity and P- and S-wave velocities.

5.8 Effect of Inclusions

Since the variations of dynamic properties (V_p , V_s , E_d and ν_d) with the variations of the physical property (ρ) and the static mechanical properties (E and ν) are due to the changes of carnallite and anhydrite contents among the salt specimens. The carnallite and anhydrite contents are therefore correlated with the previously mentioned parameters in this section. For the density, the pure carnallite and pure anhydrite have densities of 1.6 g/cc and 2.89-2.98 g/cc, respectively (Dana and Hurlbut 1948).

The specimen density can be correlated with the amount of their inclusions as:

$$\rho = 0.004 \cdot (A\% - C\%) + 2.157 \quad \text{g/cc} \quad (5.27)$$

where $A\%$ is anhydrite contents (in weight percent)

$C\%$ is carnallite contents (in weight percent)

The results show that the specimen density increases with decreasing carnallite and increasing anhydrite, as shown in Figure 5.17. Very good correlation is obtained ($R^2 = 0.976$).

The P- and S-wave velocities also vary with the carnallite and anhydrite contents as:

$$V_p = 0.022 \cdot (A\% - C\%) + 5.144 \quad \text{km/s} \quad (5.28)$$

$$V_s = 0.021 \cdot (A\% - C\%) + 2.654 \quad \text{km/s} \quad (5.29)$$

Good correlation is obtained from both wave velocities, as shown in Figure 5.18. The increase of the wave velocities is due to the increase of anhydrite and the decrease of carnallite.

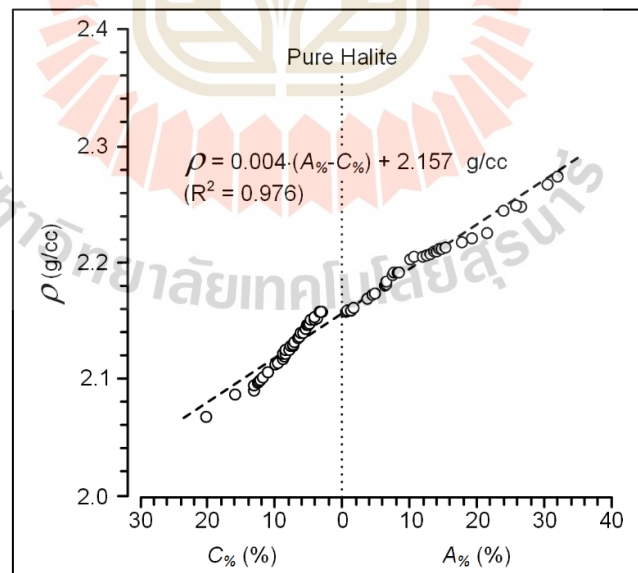


Figure 5.17 Salt specimen density as a function of carnallite and anhydrite contents.

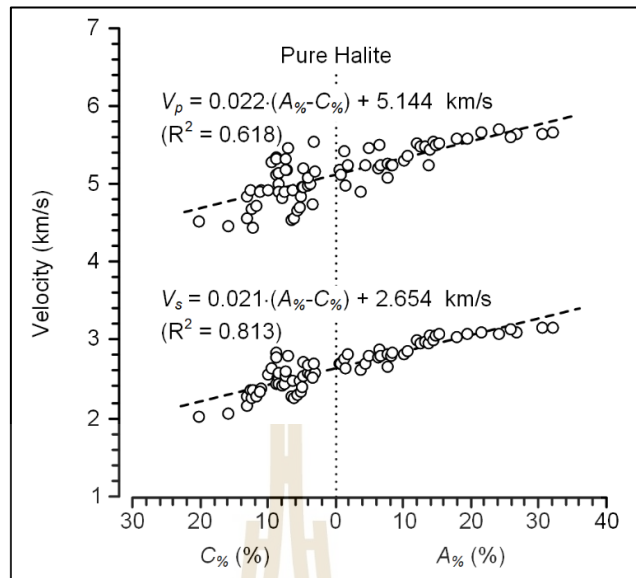


Figure 5.18 P-wave and S-wave velocities as a function of carnallite and anhydrite contents.

Similarly, the dynamic Young's modulus can be correlated with the carnallite and anhydrite contents using a linear equation, with $R^2 = 0.858$. The relationship is plotted in Figure 5.19.

$$E_d = 0.676 \cdot (A\% - C\%) + 40.493 \quad \text{GPa} \quad (5.30)$$

The dynamic Poisson's ratio (Figure 5.20) decreases with decreasing carnallite and increasing anhydrite contents.

$$\nu_d = -0.002 \cdot (A\% - C\%) + 0.318 \quad (5.31)$$

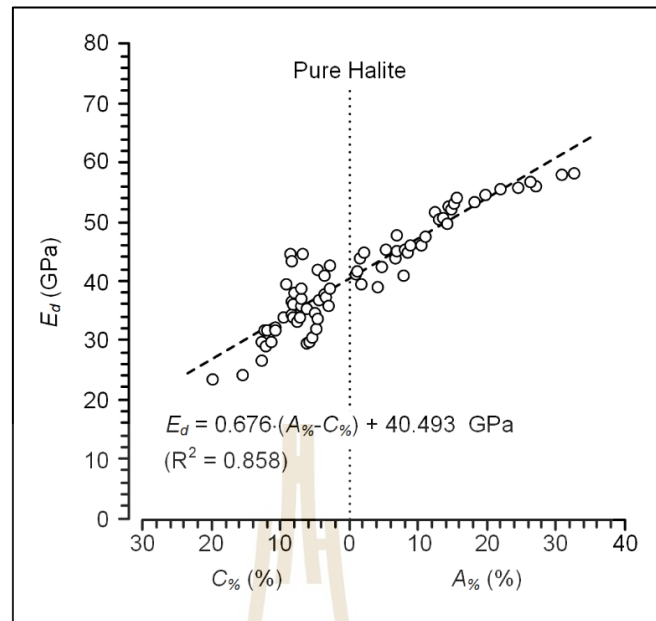


Figure 5.19 Dynamic young's modulus as a function of carnallite and anhydrite contents.

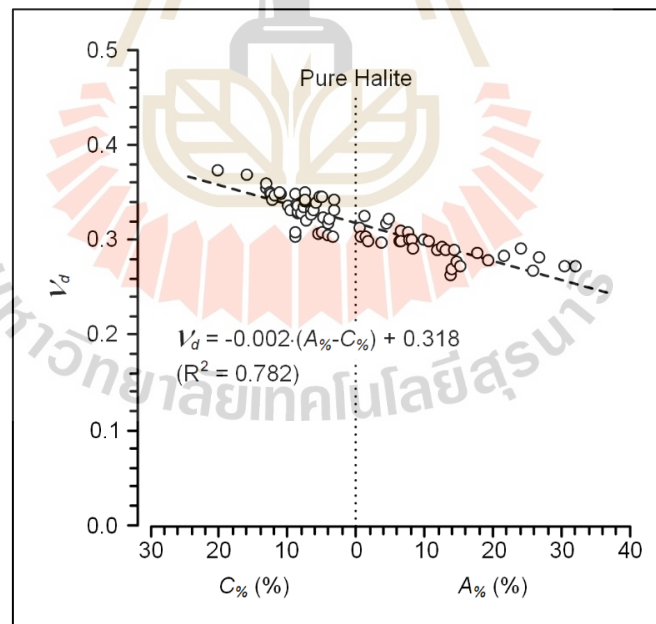


Figure 5.20 Dynamic Poisson's ratio as a function of carnallite and anhydrite contents.

For the mechanical properties, the uniaxial compressive strength, elastic modulus and Poisson's ratio can be described by the changes of carnallite and anhydrite inclusions.

Linear equation can be used to represent their relations as:

$$\sigma_c = 0.388 \cdot (A\% - C\%) + 27.58 \quad \text{MPa} \quad (5.32)$$

$$E = 0.393 \cdot (A\% - C\%) + 6.672 \quad \text{GPa} \quad (5.33)$$

$$\nu = -0.003 \cdot (A\% - C\%) + 0.308 \quad (5.34)$$

Their relationships are presented in Figures 5.21 through 5.23.

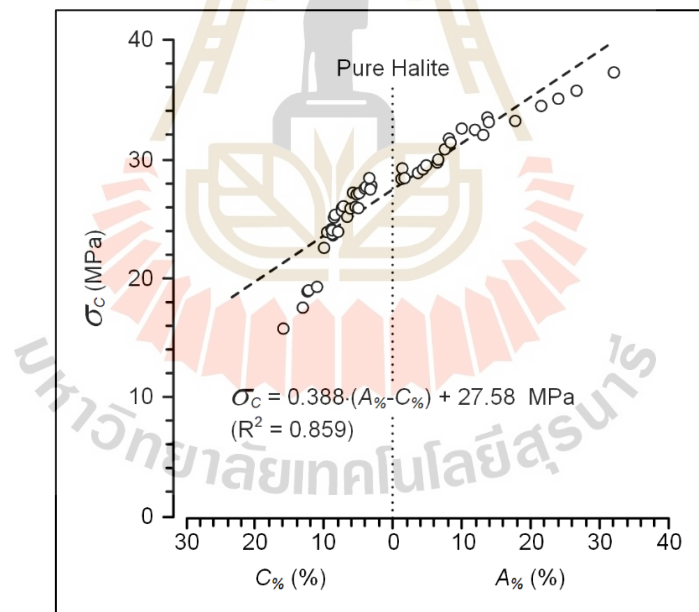


Figure 5.21 Uniaxial compressive strength as a function of carnallite and anhydrite contents.

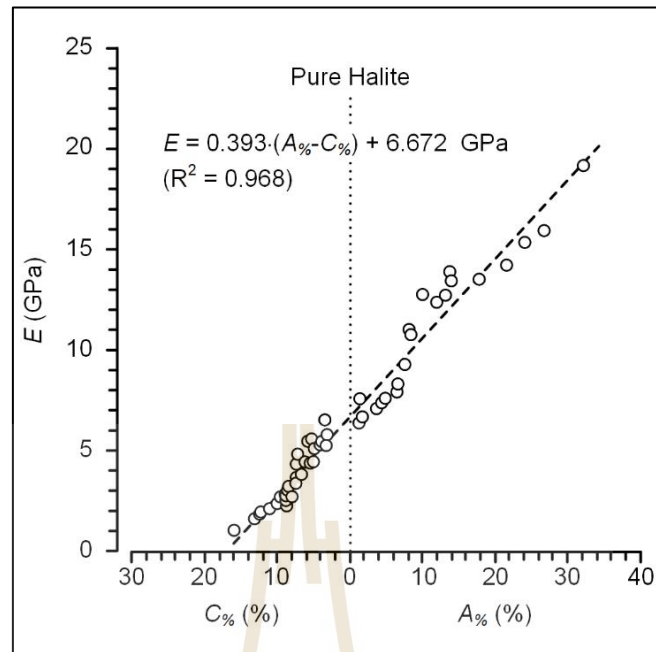


Figure 5.22 Static elastic modulus as a function of carnallite and anhydrite contents.

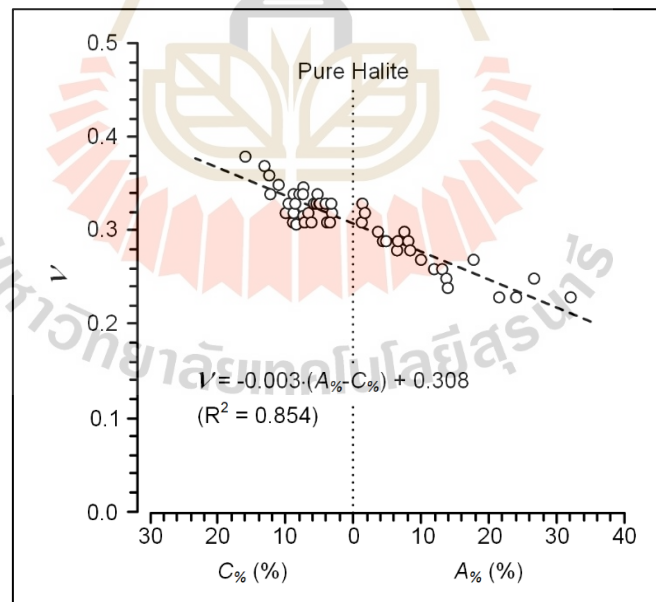


Figure 5.23 Static Poisson's ratio as a function of carnallite and anhydrite contents.

The effects of both inclusions also exhibit on the Burgers creep parameters.

Exponential equations are proposed to represent their relationships as follows:

$$E_1 = 1.056 \cdot \exp[0.041 \cdot (A\% - C\%)] \quad \text{GPa} \quad (5.35)$$

$$E_2 = 1.278 \cdot \exp[0.032 \cdot (A\% - C\%)] \quad \text{GPa} \quad (5.36)$$

$$\eta_1 = 71.115 \cdot \exp[0.066 \cdot (A\% - C\%)] \quad \text{GPa} \cdot \text{day} \quad (5.37)$$

$$\eta_2 = 3.822 \cdot \exp[0.044 \cdot (A\% - C\%)] \quad \text{GPa} \cdot \text{day} \quad (5.38)$$

Good correlations have been obtained. Figures 5.24 through 5.27 plot their relationships.

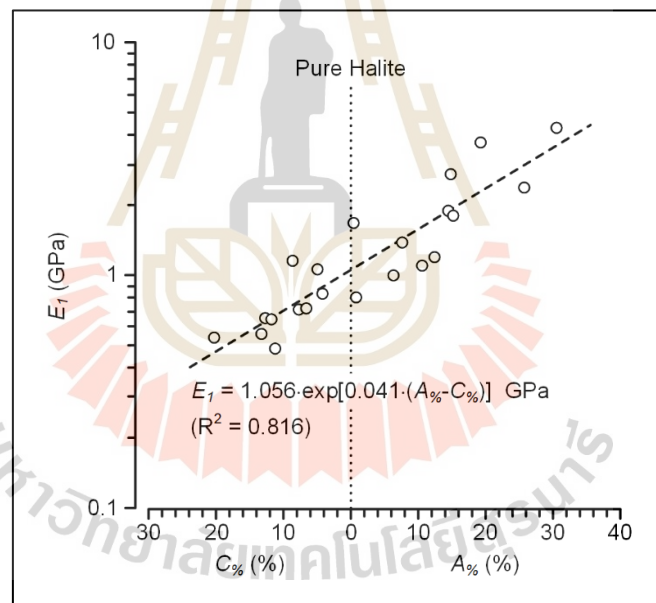


Figure 5.24 The elastic modulus as a function of carnallite and anhydrite contents.

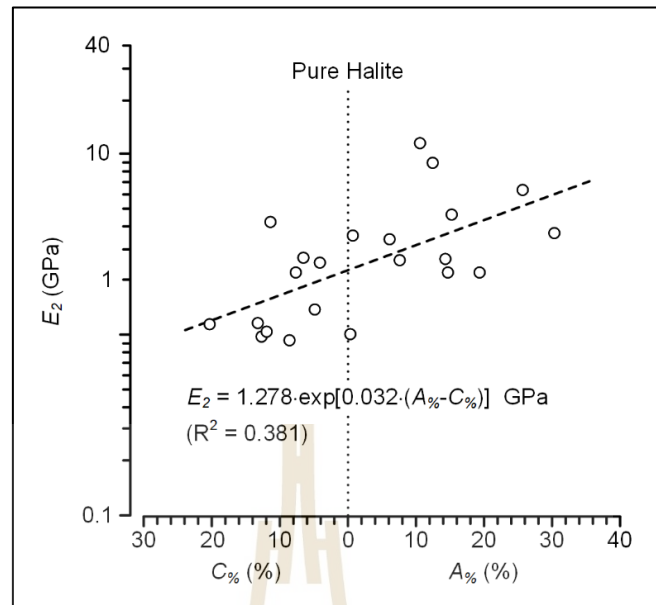


Figure 5.25 The spring constant in visco-elastic phase as a function of carnallite and anhydrite contents.

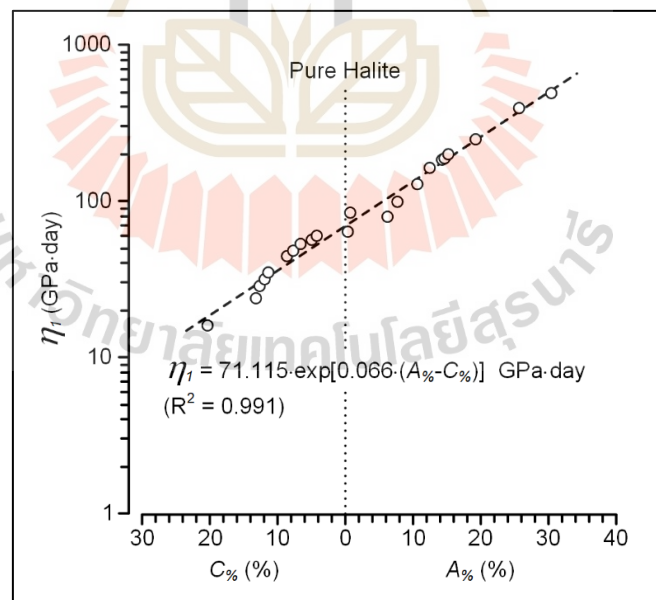


Figure 5.26 The visco-plastic coefficient as a function of carnallite and anhydrite contents.

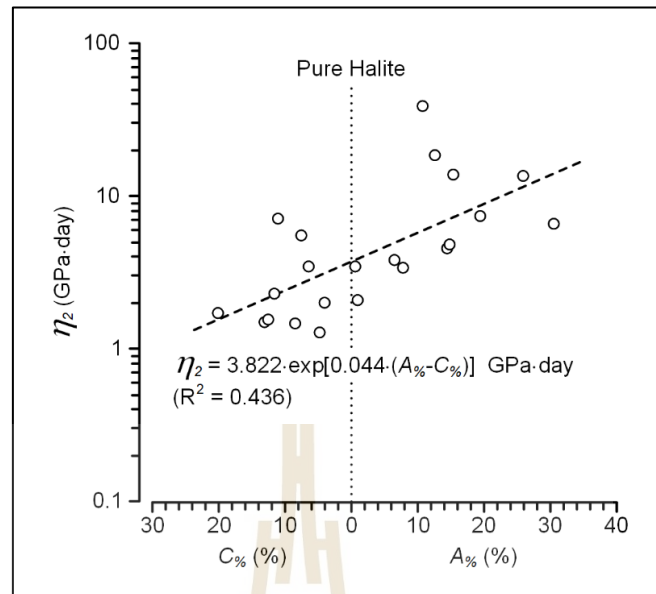


Figure 5.27 The visco-elastic viscosity as a function of carnallite and anhydrite contents.

CHAPTER VI

DISCUSSIONS AND CONCLUSIONS

6.1 Discussions

The presented study has been focused on the effects of the physical, mechanical, creep and mineral properties on the wave velocities of Maha Sarakham salt.

The densities of the tested rock salt are in the range of those tested elsewhere. The density of the samples can be distinguished clearly by P-wave and S-wave velocity which agrees with other observations (Serra, 1990; Popp et al., 2001; Jones and Davison, 2014; Zong et al., 2015). The salt specimens with carnallite inclusion have low density and low P- and S-wave velocities. The salt specimens with anhydrite inclusion have the higher density and high P- and S-wave velocities. This is because carnallite have lower specific gravity than halite and anhydrite.

Good correlations are also obtained between the specimen density and mechanical properties. The salt compressive strengths and elastic moduli increase with the specimen density (Figure 5.7 and Figure 5.8). This is because higher density specimens contain anhydrite while lower density specimens contain carnallite inclusion. Anhydrite exhibits higher strength and stiffness than carnallite (Wilalak and Fuenkajorn, 2016).

The elastic modulus increases linearly with the dynamic Young's moduli (Figure 5.11). Good correlation is obtained ($R^2 > 0.7$). Such positive relation is useful to estimate the salt stiffness from the dynamic Young's modulus. The values of the static moduli are about an order of magnitude lower than those of the dynamic properties.

This is due to the effect of loading rate. The pulse waves are much faster than those of the static loading. The Poisson's ratios obtained from the two methods are comparable (Figure 5.12).

Results from the correlations between the wave velocities and the Burgers model suggest that the long-term creep deformation of the salt containing anhydrite and carnallite inclusions can be adequately determine from the wave velocities (Figure 5.15). This could save time and effects from conducting the conventional creep testing which usually take several days. For the short-term creep deformation, relatively poor correlations are obtained (Figures 5.14 and 5.16). This may be because during the transient creep phase the salt specimens are undergone dislocation climb mechanism and elastic deformation of the inter-crystalline boundaries. Such mechanism can show high intrinsic variability, particularly for small specimen (Fuenkajorn and Daemen, 1986). Unlike the steady-state creep phase, the salt specimens are deformed smoothly under dislocation glide mechanism (sliding between cleavage planes). This explains why good correlation is obtained between the wave velocities and the visco-plastic coefficient (η_1), as shown in Figure 5.15.

The specimen compositions obtained from X-ray diffraction analysis clearly reveal the effects of the salt density on the wave velocity. Equations (5.28) and (5.29) give good transformation of the specimen properties from those with carnallite inclusions to those with anhydrite inclusions. Linear equations can adequately describe the change of the inclusion contents as affected on the static and dynamic properties of the specimens (Figures 5.17 to 5.23).

The specimens containing carnallite tend to show a higher intrinsic variability than those with anhydrite. This may be due to the fact that the anhydrite seams are more

well-defined and occur more consistently across the specimen section. While the carnallite seams are irregular and not well-defined.

Case should be taken to apply the results obtained here for engineering application. Different amounts and types of inclusions in rock salt likely result in different to correlation equations. The trace minerals inclusions are excluded from the analysis because they are relatively small amounts (less than 2%). Higher amount of trace minerals could also lead to different forms of the correlation equations.

6.2 Conclusions

Results and analysis of the ultrasonic pulse velocity measurements and mechanical and creep testing can reach conclusions as follows:

1. P- and S-wave velocities correlate fairly well with the changes of the salt specimen density using linear equations.
2. Uniaxial compressive strengths and elastic moduli show positive linear relations with the specimen densities. The specimen Poisson's ratio, however, decreases with increasing specimen density.
3. The dynamic elastic modulus are about 10 to 20 times of the static elastic modulus, primarily due to the effect of loading rate.
4. The Burgers parameters can be correlated with the wave velocities using exponential equations. Good correlations are obtained, particularly for the parameters describing the instantaneous and visco-plastic deformations. The plastic creep phase is attributed by the smooth deformation controlled by the dislocation glide mechanism (displacement of cleavage planes), and hence results in consistent $\gamma_{\text{oct}}-t$ curves.

5. The changes of the physical, mechanical and creep properties of the salt specimens can be identified by the changes of the inclusion contents with good transitions equations from those with carnallite to those with carnallite inclusions.

6.3 Recommendations for Future Studies

The uncertainties of the investigation and results discussed above lead to the recommendations for further studies as follows.

1. More testing is required on a variety of specimen densities with different inclusion contents of rock salt.
2. Increasing the number of the salt specimens would statistically enhance the predictability of the test results and the reliability of the proposed correlation equations.
3. Effects of bedding plane orientations should be studied via ultrasonic pulse velocity measurements and mechanical and creep testing.

REFERENCES

- Abdullah, N. H., Sazaly, N. N., Awang, H., and Hamid, N. H. (2019). Characterizing P-wave velocity and elastic properties of sedimentary rocks for foundation of building. **Journal of Mechanical Engineering**. 16(2): 199-210.
- Aldeeky, H. and Al Hattamleh, O. (2018). Prediction of engineering properties of basalt rock in Jordan using Ultrasonic pulse velocity test. **Geotechnical and Geological Engineering**. 36(6): 3511-3525.
- Altindag, R. (2012). Correlation between P-wave velocity and some mechanical properties for sedimentary rocks. **Journal of the Southern African Institute of Mining and Metallurgy**. 112(3): 229-237.
- Archeeploha, S., Khamrat, S., and Fuenkajorn, K. (2017). Effects of intermediate principal stress on creep closure of storage caverns in Maha Sarakham salt. **Songklanakarin Journal of Science and Technology**. 39(2): 143-151.
- ASTM D2845-08 (2008). **Standard Test Method for Laboratory Determination of Pulse Velocities and Ultrasonic Elastic Constants of Rock**. Annual Book of ASTM Standards, American Society for Testing and Materials, West Conshohocken, PA.
- ASTM D7012-14 (2014). **Standard Test Methods for Compressive Strength and Elastic Moduli of Intact Rock Core Specimens under Varying States of Stress Temperatures**. Annual Book of ASTM Standards, American Society for Testing and Materials, West Conshohocken, PA.

- ASTM D7070-08 (2008). **Standard Test Methods for Creep of Rock Core under Constant Stress and Temperature**. Annual Book of ASTM Standards, American Society for Testing and Materials, West Conshohocken, PA.
- Chary, K. B., Sarma, L. P., Lakshmi, K. P., Vijayakumar, N. A., Lakshmi, V. N., and Rao, M. V. M. S. (2006). Evaluation of engineering properties of rock using ultrasonic pulse velocity and uniaxial compressive strength. In **Proceedings of the National Seminar on Non-Destructive Evaluation, Hyderabad** (pp. 379-385). Turkey.
- Chawre, B. (2018). Correlations between ultrasonic pulse wave velocities and rock properties of quartz-mica schist. **Journal of Rock Mechanics and Geotechnical Engineering**. 10(3): 594-602.
- Dana, J. D. and Hurlbut, C. S. (1948). **Dana's manual of mineralogy**. Wiley & Sons, Incorporated.
- Fuenkajorn, K. and Daemen, J.J.K. (1986). Shape effect on ring test tensile strength. In **Proceedings of the 27th U.S. Symposium on Rock Mechanics** (pp. 155-163). Tuscaloosa: University of Alabama.
- Fuenkajorn, K. and Phueakphum, D. (2010). Effects of cyclic loading on mechanical properties of Maha Sarakham salt. **Engineering Geology**. 112(1-4): 43-52.
- Gardner, G. H. F., Gardner, L. W., and Gregory, A. R. (1974). Formation velocity and density-The diagnostic basics for stratigraphic traps. **Geophysics**. 39(6): 770-780.

- Jaroenklang, J., Chintnarin, A., Pokhee, N. and Tepnarong, P. (2017). Estimation of Mechanical Property of Carbonate Rocks Using Ultrasonic Test. In **Proceedings of the 11th South East Asean Technical University Consortium 2017 (SEATUC)**. Ho Chi Min University of Technology (HCMUT): Vietnam.
- Jones, I. F. and Davison, I. (2014). Seismic imaging in and around salt bodies. **Interpretation**. 2(4): 1-20.
- Khandelwal, M. (2013). Correlating P-wave velocity with the physico-mechanical properties of different rocks. **Pure and Applied Geophysics**. 170(4): 507-514.
- Kurtulus, C., Bozkurt, A., and Endes, H. (2012). Physical and mechanical properties of serpentinized ultrabasic rocks in NW Turkey. **Pure and Applied Geophysics**. 169(7): 1205-1215.
- Leucci, G. and De Giorgi, L. (2006). Experimental studies on the effects of fracture on the P and S wave velocity propagation in sedimentary rock ("Calcarenite del Salento"). **Engineering Geology**. 84(3-4): 130-142.
- Luangthip, A., Wilalak, N., Thongprapha, T., and Fuenkajorn, K. (2017). Effects of carnallite content on mechanical properties of Maha Sarakham rock salt. **Arabian Journal of Geosciences**. 10(6): 1-14.
- Moradian, Z. A. and Behnia, M. (2009). Predicting the uniaxial compressive strength and static Young's modulus of intact sedimentary rocks using the ultrasonic test. **International Journal of Geomechanics**. 9(1): 14-19.
- Phatthaisong, K., Sartkaew, S., and Fuenkajorn, K. (2018). Effects of loading rate and temperature on strength and deformability of Maha Sarakham salt. **Songklanakarinn Journal of Science and Technology**. 40(2):1-14.

- Popp, T., Kern, H., and Schulze, O. (2001). Evolution of dilatancy and permeability in rock salt during hydrostatic compaction and triaxial deformation. **Journal of Geophysical Research: Solid Earth**. 106(B3): 4061-4078.
- Saroglou, C. and Kallimogiannis, V. (2017). Fracturing process and effect of fracturing degree on wave velocity of a crystalline rock. **Journal of Rock Mechanics and Geotechnical Engineering**. 9(5): 797-806.
- Serra, O. (1990). **Element mineral rock catalog**. Schlumberger. 253p.
- Skrzypek, J. and Hetnarski, R. B. (1993). **Plasticity and creep theory, examples, and problems**. CRC Press, Florida. 560p.
- Song, I., Suh, M., Woo, Y. K., and Hao, T. (2004). Determination of the elastic modulus set of foliated rocks from ultrasonic velocity measurements. **Engineering Geology**. 72(3-4): 293-308.
- Teixeira, L. and Lupinacci, W. M. (2019). Elastic properties of rock salt in the Santos Basin: Relations and spatial predictions. **Journal of Petroleum Science and Engineering**. 180: 215-230.
- Vasconcelos, G., Lourenço, P. B., Alves, C. S., and Pamplona, J. (2008). Ultrasonic evaluation of the physical and mechanical properties of granites. **Ultrasonics**. 48(5): 453-466.
- Wannakhao, L., Wannakhao, P., Youngmee, W., and Rasuwan, I. (2007). The use of ultrasonic and seismic waves to evaluate engineering properties of weathered sandstones. In **Proceedings of the 1st Thailand Symposium of Rock Mechanics** (pp. 299-321). Suranaree University of Technology, Nakhon Ratchasima.

- Wannakao, L., Sriputorn, S., and Trirat, J. (2009). Correlations between mechanical and ultrasonic wave properties of claystone from Mae Moh coal mine. In **Proceedings of the 2nd Thailand Symposium of Rock Mechanics** (pp. 351-363). Suranaree University of Technology, Nakhon Ratchasima.
- Wendai, L. 2000. Regression analysis, linear regression and probity regression, In 13 chapters. SPSS for Windows: statistical analysis: Publishing House of Electronics Industry, Beijing, China.
- Wilalak, N. and Fuenkajorn, K. (2016). Constitutive equation for creep closure of shaft and borehole in potash layers with varying carnallite contents. In **Proceedings of the 9th Asian Rock Mechanics Symposium**. Bali, Indonesia.
- Zong, J., Coskun, S., Stewart, R. R., Dyaur, N., and Myers, M. T. (2015). Salt densities and velocities with application to the Gulf of Mexico salt domes. In Salt challenges in hydrocarbon exploration: In **Proceedings of the 85th Annual International Meeting**. SEG, Post-Convention Workshop.
- Zong, J., Stewart, R. R., Dyaur, N., and Myers, M. T. (2015). Elastic properties of rock salt: Lab measurements and well log analysis in the Gulf of Mexico. In **Proceedings of the Annual International Meeting** (pp. 3095-3099). SEG. Society of Exploration Geophysicists.

BIOGRAPHY

Ms. Nisachon Phongklahan was born on July 18, 1996 in Khon Kaen Province, Thailand. She received her Bachelor's Degree in Engineering (Geological Engineering) from Suranaree University of Technology in 2018. For her post-graduate, she continued to study with a Master's degree in the Geological Engineering Program, Institute of Engineering, Suranaree university of Technology. During graduation, 2018-2020, she was a part time worker in position of research assistant at the Geomechanics Research Unit, Institute of Engineering, Suranaree University of Technology.

